

# HETEROCLINIC ORBITS, MOBILITY PARAMETERS AND STABILITY FOR THIN FILM TYPE EQUATIONS

R. S. LAUGESEN AND M. C. PUGH

ABSTRACT. We study numerically the phase space of the evolution equation

$$h_t = -(h^n h_{xxx})_x - \mathcal{B}(h^m h_x)_x.$$

Here  $h(x, t) \geq 0$ ,  $n > 0$  and  $m \in \mathbb{R}$ , and the Bond number  $\mathcal{B}$  is positive.

We pursue three goals: to investigate the nonlinear stability of the positive periodic and constant steady states; to locate heteroclinic connecting orbits between these steady states and the compactly supported ‘droplet’ steady states; and to determine how these orbits change when the ‘mobility’ exponents  $n$  and  $m$  are changed.

For example, when  $n + 1 \leq m < n + 2$  we know from the companion article that there can be three fundamentally different steady states with the same period and volume. The first is a constant steady state that is a local minimum of the energy. The second is a positive periodic steady state that is a saddle for the energy and has higher energy than the constant steady state. The third is a periodic collection of droplet steady states having lower energy than either the positive or constant steady states. Here, we find numerically that the constant steady state appears to be asymptotically stable and that perturbing the positive periodic steady state in one direction yields a solution that tends to the constant steady state while perturbing in the other direction yields a solution that appears to touch down in finite time.

Also, we consider the effect of changing the mobility coefficients,  $h^n$  and  $h^m$ . We change them in such a way that the steady states are unchanged and find evidence that heteroclinic orbits between steady states are perturbed but not broken. We also find that when there appear to be touch-down singularities, the exponent  $n$  affects whether they occur in finite or infinite time. It also can affect whether there is one touch-down or two touch-downs per period.

## CONTENTS

§1, §2	—	Introduction and review of steady states
§3	—	Bifurcation diagrams and weakly nonlinear analysis
§4	—	Heteroclinic connections
§5	—	The mobility exponents
§6	—	Numerical methods
§7	—	Conclusions and future directions

## 1. INTRODUCTION

We study the evolution equation

$$(1) \quad h_t = -(h^n h_{xxx})_x - \mathcal{B}(h^m h_x)_x,$$

where  $n > 0$  and  $m \in \mathbb{R}$ , and the Bond number  $\mathcal{B} > 0$ . This is a special case in one space dimension of the equation  $h_t = -\nabla \cdot (f(h)\nabla\Delta h) - \nabla \cdot (g(h)\nabla h)$ , which has been used to model the dynamics of a thin film of viscous liquid. The air/liquid interface is at height

---

*Date:* November 15, 2018.

$z = h(x, y, t) \geq 0$  and the liquid/solid interface is at  $z = 0$ . The one dimensional equation applies if the liquid film is uniform in the  $y$  direction.

The fourth order term in equation (1) reflects surface-tension-type effects and the second order term can reflect gravity, van der Waals interactions, thermocapillary effects or the geometry of the solid substrate, for example. Typically

$$f(h) \sim h^n \quad \text{and} \quad g(h) \sim \pm \mathcal{B}h^m$$

as  $h \rightarrow 0$ , where  $1 \leq n \leq 3$  and  $m \in \mathbb{R}, \mathcal{B} > 0$ , hence our choice of  $f$  and  $g$  in (1) as power laws. See the introduction of our companion paper [19] for references to the modeling and mathematical literature.

In [18] we proved linear stability and instability results for the positive periodic steady states of (1). These results were for zero-mean perturbations that have the same period as the steady state, or shorter period — longer perturbations always lead to linear instability [18]. We summarize the linear stability and instability results in the bifurcation diagrams in §3; the main points are roughly that positive periodic steady states are linearly unstable if  $m - n < 0$  or  $m - n \geq .80$ , are linearly stable if  $0 < m - n \leq .75$  (albeit with a zero eigenvalue arising from the translation invariance of (1)), and could be either stable or unstable if  $.75 < m - n < .8$ . The case  $m - n = 0$  is degenerate.

For the linearly *stable* steady states, it is natural to ask: do numerical simulations show asymptotic stability of the steady state (modulo translation in space), meaning that a solution that starts from a perturbed steady state will relax back either to the steady state or to one of its translates? In §4.4 we show the answer is “Yes”, for  $m$  and  $n$  with  $m - n = .5$  and other values.

For the steady states  $h_{ss}$  that are linearly *unstable*, two natural questions occur. First, is the steady state *nonlinearly* unstable? We find this seems always to be the case, as evidenced by the many numerical simulations in §4. Second, do perturbations of the steady state subsequently converge to some *other* steady state, and can we predict what this long-time limiting state will be? This is a difficult question. The three most likely *candidates* for a long-time limit are: a positive periodic steady state, the constant steady state  $\overline{h_{ss}}$ , or one or more compactly supported ‘droplet’ steady states. (Droplet steady states might have zero or nonzero contact angles, but in [18, 19] we have considered only the zero contact angle case.) How can one predict which, if any, of these candidates will be the long-time limit?

One way to make predictions is by comparing the *energy levels* of these different kinds of steady state, using the energy

$$\mathcal{E}(h(\cdot, t)) = \int_0^X \left[ \frac{1}{2} h_x(x, t)^2 - \frac{\mathcal{B}}{(m - n + 2)(m - n + 1)} h(x, t)^{m-n+2} \right] dx.$$

This energy is known to be dissipated by the evolution,  $\frac{d}{dt}\mathcal{E}(h(\cdot, t)) \leq 0$ , and in our companion article [19] we proved a number of results establishing relative energy levels of positive periodic, constant and droplet steady states. For example, we proved in [19, Theorem 6] that if  $m - n < 0$  or  $m - n \geq 1$  then the positive periodic steady state  $h_{\text{ss}}$  has higher energy than the constant steady state  $\overline{h_{\text{ss}}}$ , suggesting that perturbations of  $h_{\text{ss}}$  might converge to  $\overline{h_{\text{ss}}}$ . Indeed, we find numerically in §4 for a variety of  $m$  and  $n$  values that many perturbations of  $h_{\text{ss}}$  do subsequently evolve towards the mean. In another unstable case, if  $-2 < m - n < 0$  or  $1 \leq m - n < 2$  then [19, Theorem 7] shows there is a zero angle droplet steady state with length less than the period of  $h_{\text{ss}}$ , with the same area as  $h_{\text{ss}}$ , and with less energy than  $h_{\text{ss}}$ . We find numerically in §4 that many perturbations of  $h_{\text{ss}}$  evolve towards touch-down, where the solution goes to zero at a point. Our code stops at that time, so we cannot show relaxation to the droplet steady state, but this certainly seems a likely eventual outcome.

Our theorems and simulations thus allow us to predict at least a couple of likely long-time limits. But when there is more than one steady state with lower energy than  $h_{\text{ss}}$ , we have not been able to predict to where a given perturbation of  $h_{\text{ss}}$  will relax. And we are so far unable to predict the amount of translation that might occur in the long-time limit (for example, where will the maximum of the limiting steady state occur?). Impressive results on such a translation problem have recently been obtained by [11] for the Cahn–Hilliard equation  $h_t = -h_{xxxx} - ((1 - 3h^2)h_x)_x$  on the whole real line.

In this paper we also ask how the evolution is affected by changes in the coefficient functions  $h^n$  and  $h^m$ . In particular, we consider the evolution of a fixed initial condition under the equation (1) for two different pairs  $(n_1, m_1)$  and  $(n_2, m_2)$  of exponents. One can show that the steady states of the two evolution equations are the same if  $m_1 - n_1 = m_2 - n_2$ . In that case we ask: given the same initial data, do the two solutions have the same long-time limit? Or, can changing the mobility exponents  $n$  and  $m$  can change the long-time limit? We also ask whether changing the mobility parameters can affect the number and type of finite-time singularities.

Before outlining the paper, we note that throughout the paper we consider only *zero-mean* perturbations. This seems reasonable from a physical standpoint, because such perturbations correspond to a disturbance of the fluid that alters the profile without adding additional fluid. Mathematically it is reasonable because the evolution equation (1) preserves volume for spatially periodic solutions:  $\int h(x, t) dx = \int h(x, 0) dx$  for all time  $t$ . Thus zero-mean perturbations allow the possibility of relaxation back to the original steady state, while nonzero-mean perturbations do not.

**Outline of the paper.** This paper reports on numerical simulations that are inspired by, and extend, the theoretical results in our linear stability paper [18] and our companion

paper [19] on energy stability and relative energy levels of steady states. The stability results of [18, 19] are summarized by the bifurcation diagrams in §3 below, and we will remind the reader of the relevant results and their implications when describing our numerical simulations. So the reader need not digest the earlier papers [18, 19] before reading this one, although it would help to have those papers at hand.

The bifurcation diagrams in Section 3 summarize the known results from [18, 19] on stability of steady states. The section also contains a weakly nonlinear stability analysis.

Section 4 presents a detailed numerical study of the evolution equation (1), for a number of different exponents  $n$  and  $m$ . We focus especially on initial data close to a steady state. Our stability and energy level results from [18, 19] lead to many predictions for the behavior of the solution, both short and long time, and these predictions are generally borne out by our simulations. Strikingly, the period and area of the initial data, the Bond number  $\mathcal{B}$  and the value  $m - n$  seem to be sufficient information to reduce the possible long-time behavior to just a couple of options.

We find evidence for heteroclinic connections between different types of steady state (such as: periodic to constant, periodic to droplet, and constant to droplet). One would like to know how robust the behaviors observed in our numerical simulations are under changes in the coefficients  $h^n$  and  $\mathcal{B}h^m$ . In particular, what happens when the mobility exponents  $n$  and  $m$  are changed in a way that  $n - m$  is unchanged, leaving the steady states of the evolution unchanged? In Section 5.1 we give numerical evidence that such changes perturb, but do not break, heteroclinic orbits.

Another question investigated in Section 5 is how changing  $m$  and  $n$  affects singularity formation. For the equation  $h_t = -(h^n h_{xxx})_x$ , there has been extensive computational work studying how the choice of  $n$  affects the spatial structure of singularities and whether they occur in finite or in infinite time [5]. Specifically, simulations suggest there is a critical exponent  $1 < n_c < 2$  such that if  $n > n_c$  then solutions are positive for all time while solutions can touch down in finite time if  $n < n_c$ . For our equation (1), we numerically estimate  $n_c$  in §5.2. We find that its value depends on the difference  $m - n$ . Then in §5.3, we demonstrate that the mobility can also affect the *number* of apparent singularities per period.

Section 6 discusses our numerical methods.

Section 7 sums up the paper, and recalls the ‘gradient flow for the energy’ interpretation of the evolution equation (1).

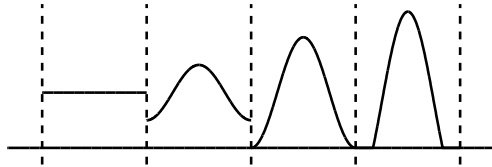


Figure 1: Four types of steady state.

## 2. TERMINOLOGY, DEFINITION OF THE ENERGY, AND REVIEW OF STEADY STATES

**Terminology.** We write  $\mathbb{T}_X$  for a circle of circumference  $X > 0$ . As usual, one identifies functions on  $\mathbb{T}_X$  with functions on  $\mathbb{R}$  that are  $X$ -periodic and calls them *even* or *odd* according to whether they are even or odd on  $\mathbb{R}$ .

Positive periodic steady states are assumed to satisfy the steady state equation classically. A droplet steady state  $h_{\text{ss}}(x)$  (see Figure 1) is by definition positive on some interval  $(a, b)$  and zero elsewhere, with  $h_{\text{ss}} \in C^1[a, b]$ ; we require  $h_{\text{ss}}$  to satisfy the steady state equation classically on the open interval  $(a, b)$ , and to have equal acute contact angles:  $0 \leq h'_{\text{ss}}(a) = -h'_{\text{ss}}(b) < \infty$ . (Throughout the paper, if a function has only one independent variable then we use  $'$  to denote differentiation with respect to that variable:  $h'_{\text{ss}} = (h_{\text{ss}})_x$ .)

We say a droplet steady state  $h_{\text{ss}}$  has ‘zero contact angle’ if  $0 = h'_{\text{ss}}(a) = -h'_{\text{ss}}(b)$ , and ‘nonzero contact angle’ otherwise. A ‘configuration’ of droplet steady states is a collection of steady droplets whose supports are disjoint.

**Definition of the energy.** There is a well-known dissipated energy (or Liapunov function) for the evolution equation (1). It is defined for  $\ell \in H^1(\mathbb{T}_X)$  to be

$$(2) \quad \mathcal{E}(\ell) = \int_0^X \left[ \frac{1}{2}(\ell')^2 - H(\ell) \right] dx,$$

where  $H$  is a function with  $H''(y) = \mathcal{B}y^{m-n}$ . This energy is strictly dissipated: if  $h(x, t)$  is a smooth solution of (1) then  $(d/dt)\mathcal{E}(h(\cdot, t)) \leq 0$ , with equality if and only if  $h$  is a steady state (cf. [19, §2.1]). The energy, like the evolution equation, is invariant under translation: hence it cannot distinguish between a steady state and its translates.

A precise definition of linear stability can be found in [18, Appendix A], and of energy stability in [19, §2], but those definitions are not needed to understand this paper.

**Brief review of steady states.** Here we quickly review the basic facts about steady states needed to appreciate this paper. For more on the steady states and their properties, and for justifications of the following remarks, see [19, §2.3] and [17] and the references therein.

We start with a non-constant positive periodic steady state  $h_{\text{ss}} \in C^4(\mathbb{T}_X)$  of the evolution (1). We translate  $h_{\text{ss}}$  so that its minimum occurs at  $x = 0$ . The steady state equation for (1) integrates to give  $h_{\text{ss}}^n h_{\text{ss}}''' + \mathcal{B}h_{\text{ss}}^m h_{\text{ss}}' = C$  for some constant  $C$ .

The constant  $C$  (the flux) equals zero, by integrating  $h_{\text{ss}}''' + \mathcal{B}h_{\text{ss}}^{m-n}h_{\text{ss}}' = Ch_{\text{ss}}^{-n}$  over a period. Hence the steady state satisfies

$$(3) \quad h_{\text{ss}}''' + r(h_{\text{ss}})h_{\text{ss}}' = 0;$$

here  $r(y) := \mathcal{B}y^{q-1}$  and

$$\boxed{q := m - n + 1.}$$

This exponent  $q$  determines many properties of the steady state, including (usually) its linear stability.

Integrating, we find the steady states have a nonlinear oscillator formulation:

$$(4) \quad h_{\text{ss}}'' + \frac{\mathcal{B}h_{\text{ss}}^q - D}{q} = 0$$

for some constant  $D$ , when  $q \neq 0$ . For  $q = 0$  the analogous equation is  $h_{\text{ss}}'' + \mathcal{B} \log h_{\text{ss}} - D = 0$ . This oscillator equation contains three constants:  $q$ ,  $\mathcal{B}$ , and  $D$ , but  $\mathcal{B}$  and  $D$  can be removed by rescaling  $h_{\text{ss}}$  and  $x$  (see [19, eq. (7)]), leading to the ‘canonical’ steady state equation

$$(5) \quad k'' + \frac{k^q - 1}{q} = 0, \quad q \neq 0,$$

$$(6) \quad k'' + \log k = 0, \quad q = 0.$$

Every positive periodic steady state  $h_{\text{ss}}$  can be rescaled to such a function  $k = k_\alpha$  with  $k'_\alpha(0) = 0$ , where we write  $\alpha = k(0) \in (0, 1)$  for the initial value. Conversely, for each  $q \in \mathbb{R}$  and  $\alpha \in (0, 1)$  there exists a unique smooth positive periodic  $k_\alpha$  satisfying equations (5–6) and with  $k_\alpha(0) = \alpha, k'_\alpha(0) = 0$ . The same holds for  $\alpha = 0$  when  $q > -1$ , although  $k_0$  may be only  $C^1$ -smooth at  $x = 0$ , where  $k_0(0) = 0$  (see [17, Theorem 3.2]).

We write

$$P = P_\alpha = P(\alpha) \quad \text{and} \quad A = A_\alpha = A(\alpha)$$

respectively for the least period of  $k_\alpha$  and for the area under its graph,  $A = \int_0^P k_\alpha(x) dx$ . Note that  $P_\alpha$  and  $A_\alpha$  approach  $2\pi$  as  $\alpha \rightarrow 1$ . As seen in [18, 19], the function

$$E(\alpha) := P(\alpha)^{3-q}A(\alpha)^{q-1} = P(\alpha)^2[A(\alpha)/P(\alpha)]^{q-1}$$

plays a large role in the stability theory of the steady states, in part due to its rescaling invariance:

$$(7) \quad \mathcal{B}P_{\text{ss}}^{3-q}A_{\text{ss}}^{q-1} = P(\alpha)^{3-q}A(\alpha)^{q-1} (= E(\alpha)),$$

where  $P_{\text{ss}}$  and  $A_{\text{ss}}$  are the period and area of the steady state  $h_{\text{ss}}$ .

### 3. BIFURCATION DIAGRAMS AND WEAKLY NONLINEAR ANALYSIS

In this section we present bifurcation diagrams that encode the linear stability information in [18, 19]. Then we relate our bifurcation diagrams to a weakly nonlinear analysis near the constant steady state.

**3.1. Bifurcation diagrams.** Figure 2 gives bifurcation diagrams for various values of  $q$ . These  $q$ -values are representative members of the intervals  $(-\infty, 1)$ ,  $(1, 1.75)$ ,  $(1.75, 1.794)$ , and  $(1.795, \infty)$ . (The value 1.794 approximates a critical exponent; see [17, §5.1] for further details.)

In all these diagrams we are considering the  $2\pi$ -periodic problem with  $\mathcal{B} = 1$ . We construct the diagrams as follows. Given  $q$ , we first compute the rescaled steady states  $k_\alpha$  for a range of  $\alpha \in (0, 1)$ . For each  $k_\alpha$ , we use its period  $P_\alpha$  to determine a constant  $D$  in the rescaling [19, eq. (7)] that yields a positive steady state  $h_{ss}$  of period  $P_{ss} = 2\pi$ . We then plot the amplitude of  $h_{ss}$  versus the scale invariant quantity  $E = \mathcal{B}P_{ss}^{3-q}A_{ss}^{q-1}$ , determining the linear stability of the steady state by the results in [18, §3.2], particularly [18, Theorem 9]. The conclusions on linear stability summarized in the figure are rigorously proved in [18] except for  $1 < q < 2$ , in which case we are relying on a combination of analytical and numerical results.

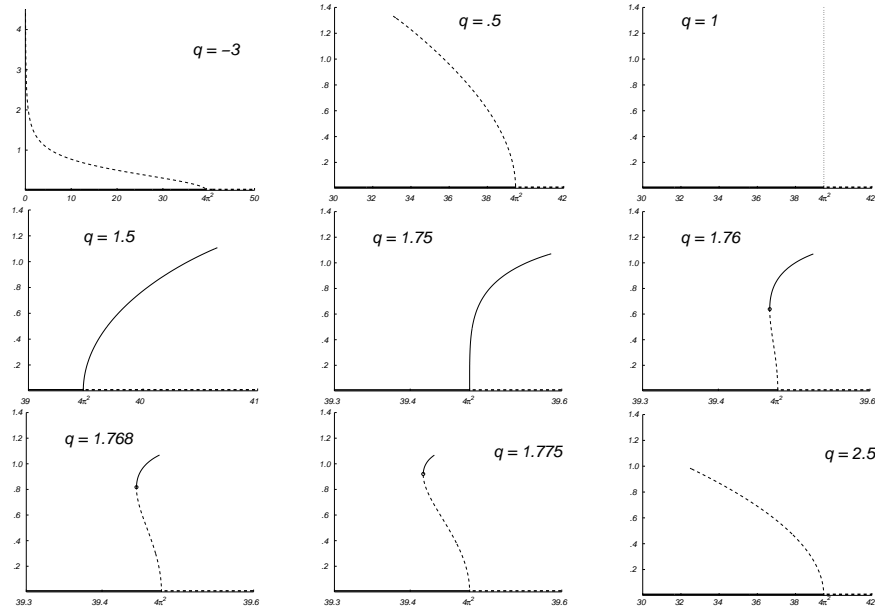


Fig.2: The  $x$ -axis is  $\mathcal{B}P_{ss}^{3-q}A_{ss}^{q-1}$  and  $y$ -axis is  $(h_{max} - h_{min})/2$ . Dashed: linearly unstable; dotted: linearly neutrally stable; solid: linearly stable.

The horizontal axes of these diagrams also show the linear stability of the *constant* steady state, with respect to zero-mean perturbations, where the constant steady state is considered as having period  $P_{ss}$  and area  $A_{ss}$ . This linear stability information is taken from [19, Theorem 10].

Qualitatively, the diagrams change continuously as  $q$  increases. Choosing a period other than  $2\pi$  or a Bond number other than  $\mathcal{B} = 1$  simply dilates the  $y$ -axis of the diagrams. We discuss the diagrams further when we present numerical simulations in §4.

**3.2. Weakly nonlinear analysis.** In the following, we sketch the weakly nonlinear analysis for the evolution equation (1). This was done for  $q = -3$  in [26, §2.3].

In short, we consider physical parameters such that the constant steady state has one mode which is barely linearly stable or is barely linearly unstable, while all other modes are strongly damped. This yields a separation of timescales which allows one to find a reduced representation of the PDE in terms of an ODE governing the amplitude of the unstable mode. We refer the reader to §5.1 of [20].

Let  $h$  be an  $X$ -periodic solution of  $h_t = -(h^n h_{xxx})_x - \mathcal{B}(h^m h_x)_x$  with mean value  $\bar{h}$ . We rescale the solution to have period  $2\pi$  and mean value 1, and we also rescale time:

$$\zeta = \frac{2\pi x}{X}, \quad \bar{h}\eta = h, \quad \text{and} \quad t' = \left(\frac{2\pi}{X}\right)^2 t.$$

The rescaled evolution equation is  $\eta_{t'} = -\sigma(\eta^n \eta_{\zeta\zeta\zeta})_{\zeta} - \mu(\eta^m \eta_{\zeta})_{\zeta}$  where

$$\sigma = \left(\frac{2\pi}{X}\right)^2 \bar{h}^n \quad \text{and} \quad \mu = \mathcal{B}\bar{h}^m.$$

Linearizing about  $\bar{h} = 1$ , we find that linearly unstable modes exist if  $0 < k < k_c$ . Proceeding in the usual manner, we introduce a small parameter  $\delta$  that corresponds to moving through the critical wave number  $k_c = 1$ :

$$\frac{\mu}{\sigma} = 1 + Q\delta^2$$

where  $Q = \pm 1$ . We then introduce a slow time-scale  $\tau = \delta^2 t'$  and expand the solution in orders of  $\delta$ :  $\eta(\zeta, \tau) = 1 + \delta\eta_1(\zeta, \tau) + \delta^2\eta_2(\zeta, \tau) + \delta^3\eta_3(\zeta, \tau) + O(\delta^4)$ . For simplicity, we assume the solution is even. By the usual arguments,  $\eta_1(\zeta, \tau) = A(\tau) \cos(\zeta)$ ,  $\eta_2(\zeta, \tau) = B(\tau) \cos(2\zeta)$ , and  $\eta_3(\zeta, \tau) = C(\tau) \cos(3\zeta)$ . Putting this ansatz into the evolution equation and expanding in orders of  $\delta$ , we find there are no  $O(1)$  or  $O(\delta)$  terms. At  $O(\delta^2)$  and  $O(\delta^3)$ , one determines the amplitudes  $B(\tau)$  and  $C(\tau)$  in terms of  $A(\tau)$  which, in turn, satisfies

$$\frac{dA}{d\tau} = Q\sigma A(\tau) - \kappa A(\tau)^3 \quad \text{where} \quad \kappa = \frac{\sigma}{6}(q-1)(1.75-q).$$

The dynamics of the amplitude  $A(\tau)$  depend on the signs of the Landau constant  $\kappa$  and of the linear term. If  $\kappa > 0$  then for  $Q = 1$  the constant  $A(\tau) \equiv 0$  is linearly unstable and  $A(\tau)$  saturates to the linearly stable amplitude  $A_c(\tau) \equiv \sqrt{\sigma/\kappa}$ . This corresponds to a supercritical bifurcation. If  $\kappa < 0$  then for  $Q = -1$  the constant  $A(\tau) \equiv 0$  is linearly stable and the steady amplitude  $A_c(\tau) \equiv \sqrt{-\sigma/\kappa}$  is linearly unstable. This corresponds to a subcritical bifurcation. Since  $\sigma > 0$ ,

$$1 < q < 1.75 \implies \text{supercritical bifurcation} \quad \text{and} \quad q < 1, 1.75 < q \implies \text{subcritical bifurcation}.$$

The Landau constant  $\kappa$  is determined by the mean value  $\bar{h}$ , the period  $X$ , and the exponents  $m$  and  $n$ , but not the Bond number  $\mathcal{B}$ . Subcritical bifurcations are often seen in systems that can have finite-time pinching (rupture) singularities *e.g.* [4, §3.2], [21, §IV].

The above weakly nonlinear analysis is consistent with our analytical and computational results. Specifically, recalling the bifurcation diagrams in Figure 2 we note that positive periodic steady states are linearly unstable for  $q < 1$  and  $q \geq 2$ . For  $1.75 < q < 2$ , when there is only one positive periodic steady state it is linearly unstable. When there are two, the one of smaller amplitude  $(h_{max} - h_{min})/2$  is linearly unstable. For  $1 < q \leq 1.75$  the positive periodic steady state is linearly stable.

#### 4. SIMULATIONS, AND HETEROCLINIC ORBITS CONNECTING STEADY STATES

We now numerically simulate solutions of the evolution equation (1), for a wide range of initial data near steady states. This has not been done before. The solutions obtained display a great variety of stability and long-time behaviors. Our stability theorems [18, 19] often allow us to *predict* the numerically observed short-time behavior, and our theorems on the energy levels of steady states [19] often allow us to guess the long-time limit of the evolution. As part of this we predict (and find strong evidence for) heteroclinic connections between certain steady states.

We expect our numerical investigations of the power law evolution (1) will provide resources, ideas and motivation for researchers studying  $h_t = -(f(h)h_{xxx})_x - (g(h)h_x)_x$  with non-power law coefficient functions  $f$  and  $g$ . There are some such numerical studies already. For example, the papers [15, 21] consider an  $f$  that is degenerate ( $f(0) = 0$ ) and  $g$ 's that are not power laws, and there is a large literature on the Cahn–Hilliard equation (for which  $f \equiv 1$  and  $g$  is a quadratic).

Recall the steady states depend on the parameter

$$q = m - n + 1.$$

We take seven values of  $q$ :

$$q = -3, 0.5, 1, 1.5, 1.768, 2.5, 4,$$

representatives of the intervals  $\{(-\infty, -1], (-1, 1), (1, 1.75], (1.75, 1.79), (1.8, 3), [3, \infty)\}$  in which our theorems suggest the solutions will display distinct behaviors. For the  $q = -3$  case, we take  $n = 3$  and  $m = -1$ , making (1) a ‘van der Waals’ equation previously studied by other authors. Otherwise, we take  $n = 1$  and  $m = q$ . In any event, we find in §5 that our numerical simulations are not greatly affected if we change  $n > 0$  and  $m$  in a manner that keeps  $q$  fixed (*i.e.* that keeps  $m - n$  fixed).

#### 4.1. $q = -3$ : the van der Waals case.

*Characteristic features for  $q \in (-\infty, -1]$ : positive periodic steady states are linearly unstable, and there are no droplet steady states with acute contact angles.* (See bifurcation diagram 2a and [17, §2.2].)

4.1.1.  $q = -3$ . *Perturbing the positive periodic steady state.* First we explain how to find a steady state having period  $P_{ss} = 2\pi$  and having some specified value for the area (or volume)  $A_{ss} = \int_0^{2\pi} h_{ss}(x) dx$ .

Given the Bond number  $\mathcal{B}$  (a physical parameter), a positive steady state satisfies (4):

$$h_{ss}'' + \frac{\mathcal{B}h_{ss}^q - D}{q} = 0$$

for some constant  $D$ . The problem is to find the value of  $D$  for which there is a steady state of period  $2\pi$  and area  $A_{ss}$ . For  $q \leq -1$ , if  $A_{ss} > 2\pi \mathcal{B}^{1/(1-q)}$  then there exists a non-constant positive periodic steady state  $h_{ss}$  with period  $2\pi$  and area  $A_{ss}$  (see [17, §5.1]). The rescaling [19, eq. (7)] then implies there is an admissible value of  $D$ .

For simplicity, instead of starting with the Bond number  $\mathcal{B}$  and finding this admissible values of  $D$ , we instead fix  $D = 1$  and determine the interval of admissible  $\mathcal{B}$  values. That is, we choose  $\alpha \in (0, 1)$  and consider the steady state  $k_\alpha$  of the rescaled equation, as in §2. Its period  $P(\alpha)$  together with  $D = 1$  and  $P_{ss} = 2\pi$  then uniquely determine  $\mathcal{B}$  by [19, eq. (24)], and hence the steady state  $h_{ss}$  by [19, eq. (7)]. (Choosing a different  $\alpha$  would yield a different  $\mathcal{B}$  and  $h_{ss}$ .) Finally, we locate a nearby ‘finite-difference steady state’ on  $N$  meshpoints (see §6.3) and study numerically its stability under perturbation.

For  $q = -3$  we carry out this construction with  $\alpha = 0.2145$  and period  $P_\alpha = 16.32$ , resulting in Bond number  $\mathcal{B} = 0.003259$ , and a non-constant positive periodic finite-difference steady state  $h_{ss}$  of least period  $2\pi$  and with area  $A = 6.884$ . Note the positive periodic steady state is linearly unstable, by bifurcation diagram 2a with  $\mathcal{B}P_{ss}^{3-q}A_{ss}^{q-1} = .08930$ .

**Remark:** For the rest of §4, whenever we refer to a ‘positive periodic steady state’, we implicitly mean a  $2\pi$ -periodic *finite-difference steady state* that has its minimum at  $x = 0$  (see §6.3). Also, we always find our periodic steady states as above, by fixing  $D = 1$  then choosing  $\alpha \in (0, 1)$  and then determining  $\mathcal{B}$  and  $A_{ss}$ . The only exception is for the  $q = 1.768$  simulations discussed in §4.5.

Now that we have a steady state for  $q = -3$ , we use a perturbation of it as initial data in the equation

$$(8) \quad h_t = -(h^3 h_{xxx})_x - \mathcal{B}(h^{-1} h_x)_x.$$

Here  $n = 3, m = -1$  and  $q = m - n + 1 = -3$ . We study this equation for the rest of §4.1. It was proposed by Williams and Davis [24] to model a thin liquid film with net repulsive

van der Waals interactions, and more recently it has been studied by Zhang and Lister [27] and by Witelski and Bernoff [25, 26].

- *Even perturbations.*

First we perturb  $h_{\text{ss}}$  with the even zero-mean perturbation  $\pm\varepsilon h_{\text{ss}}''$  and numerically study the resulting solution.

The steady state  $h_{\text{ss}}$  is linearly unstable and since the perturbation  $+\varepsilon h_{\text{ss}}''$  lowers the maximum of  $h_{\text{ss}}$  and raises the minimum, one might hope the resulting solution would converge to the constant steady state  $h \equiv \overline{h_{\text{ss}}}$ . If this happens for all small  $\varepsilon$ , then this would be strong evidence for existence of a heteroclinic orbit connecting  $h_{\text{ss}}$  to the constant steady state. There are a number of theoretical reasons to suspect such heteroclinic orbits exist: (i)  $h_{\text{ss}}$  is energy unstable in the directions  $\pm h_{\text{ss}}''$  by [19, Theorem 2], (ii) the energy of  $h_{\text{ss}}$  is higher than that of the constant steady state  $\overline{h_{\text{ss}}}$  by [19, Theorem 6] (also observed numerically by Witelski and Bernoff [26, §3]), and (iii) the constant steady state is a local minimum of the energy  $\mathcal{E}$  by [19, Theorem 10]. [To deduce (iii) from [19, Theorem 10] requires  $\mathcal{B}\overline{h_{\text{ss}}}^{q-1}X^2 < 4\pi^2$ , which we now establish:  $\mathcal{B}\overline{h_{\text{ss}}}^{q-1}X^2 = \mathcal{B}X^{3-q}A_{\text{ss}}^{q-1} = E(\alpha)$  for some  $\alpha \in (0, 1)$ , by rescaling as in (7), and  $E(1) = 4\pi^2$ . So we want to show  $E(\alpha) < E(1)$ ; this holds because  $E' > 0$  by [18, Theorem 11], since  $q < 1$ .]

To seek evidence for a heteroclinic connection, we start with initial data  $h_{\text{ss}} + 10^{-4}h_{\text{ss}}''$ . Here, we've normalized  $h_{\text{ss}}''$  to have  $L^\infty$  norm 1; all perturbations are similarly normalized. We have also considered  $\varepsilon$  smaller than  $10^{-4}$ , in most of the simulations below; we found that these smaller perturbations resulted in qualitatively the same behavior, until one hits the level of roundoff error.

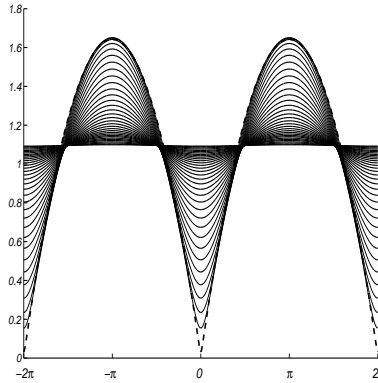


Fig.3:  $q = -3, n = 3$ . Dashed: initial data  $h_{\text{ss}} + 10^{-4}h_{\text{ss}}''$ . Local extrema stay fixed in space and solution relaxes to the mean.

The steady state  $h_{\text{ss}}$  has very large curvature at its local minima, and so we need a large number of meshpoints to resolve the initial data  $h_{\text{ss}} + 10^{-4}h_{\text{ss}}''$  with spectral accuracy. We find that for a solution on  $[0, 2\pi)$  we need 2048 meshpoints:  $h_{\text{ss}}(x) = \sum_{k=-1023}^{1023} a_k \exp(ikx)$

has amplitudes that decay to the level of round-off error ( $a_k \sim 10^{-13}$  for  $k \sim 1024$ ). Figure 3 shows the evolution of the solution; the solution relaxes to the constant steady state. (This was shown previously in [26, Figure 4b].) We use the adaptive timestepping described in §6.2. At first sight, this would seem unnecessary since the solution is becoming more regular as it evolves. However, there is a short transient during which  $h_{min}(t)$  decreases. The timestep initially decreases to accurately track this fast behavior and then increases as the solution relaxes to the mean. We use adaptive time-stepping throughout our work since we almost always observe such a short transient. Also, in a number of cases, the solutions become less smooth (curvatures increase) as time passes, requiring refinement later in time.

In the opposite direction, the perturbation  $-\varepsilon h''_{ss}$  raises the maximum and lowers the minimum of the steady state  $h_{ss}$ . Since  $h_{ss}$  is energy unstable, we might expect the solution to subsequently converge to a droplet steady state or to a configuration of droplet steady states. From [17, §2.2], if such a droplet exists it must have  $90^\circ$  contact angles, though we have not discussed such steady states here in this paper or in [17, 18].

Our numerical simulation of the solution with initial data  $h_{ss} - 10^{-4}h''_{ss}$  shows that, after a short transient, the minimum height of the solution decreases in time, appearing to decrease to zero in finite time. As the minimum height decreases, the curvature increases, requiring that after some time the number of meshpoints be increased to keep the solution spectrally resolved. We do this as follows. We compute the solution with 2048 meshpoints until the computation stops ( $h_{min}(t) = 0$ , see §6.4.) We look at the power spectrum of the solution and choose a time right before the active part of the power-spectrum is reaching the Nyquist frequency (see right plot of Figure 5). That is, we find the last time at which the 1023rd Fourier amplitude of the solution is at the level of round-off. We take the solution at this time and compute its Fourier coefficients, defined for wave numbers  $-N/2 + 1 \leq k \leq N/2 - 1$  where  $N = 2048$ . We pad by zeros, extending the Fourier coefficients to be defined for wave numbers  $-N + 1 \leq k \leq N - 1$ , and then compute the inverse Fourier transform. This yields a function on  $2N$  meshpoints that is indistinguishable from the solution at that time, to the level of round-off. Using this function as initial data, we continue the computation on  $2N$  meshpoints, repeating this point-doubling process whenever the solution becomes unresolved.

In this way, we computed a resolved solution to time  $t = .0472496406249$ , the time when the 32,768 meshpoint solution became unresolved. The top left plot in Figure 4 presents the evolution of the solution near  $x = 0$ . As before, the local extrema are fixed in space, with the solution appearing to touch down at one point per period. (This was shown previously in [26, Figure 4c].) We did not design the code to study the formation of finite-time singularities; the solution has decreased by only a factor of 6.04 due to limitations of our uniform-mesh code (see §6.4). Computing the derivative  $h_x$  of the solution, we find that its maximum

and minimum values grow as time passes, as in the bottom left plot of Figure 4. These extremum points of  $h_x$  move in time, appearing to converge to  $x = 0$  as the singular time approaches. This is consistent with a solution that touches down with  $90^\circ$  contact angles in finite time. The right plots in Figure 4 show the final resolved solution, which suggests  $90^\circ$  contact angles are developing.

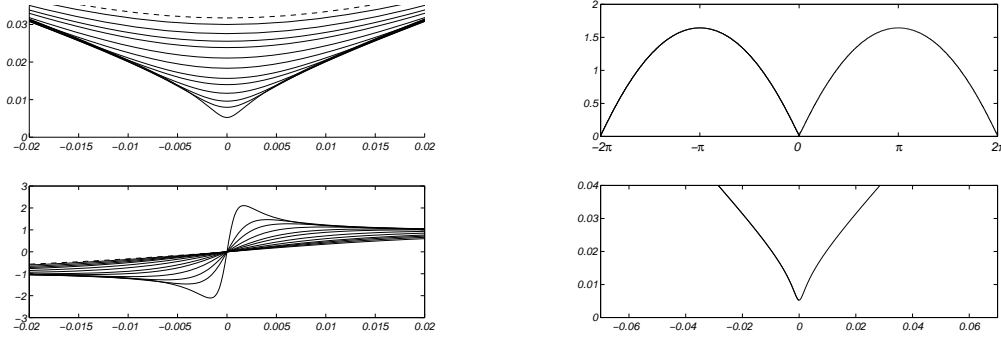


Fig.4: Left top: dashed line, initial data  $h_{ss} - 10^{-4}h''_{ss}$ ; solid lines, solution  $h$  at later times. Local minimum is fixed in space and decreases monotonically after short transient. Left bottom: dashed line, initial slope; solid lines,  $h_x$  at same times as above ( $\|h_x\|_\infty$  increases in time). Right top: solution at final resolved time,  $t = .0472496406249$ . Right bottom: close-up near  $x = 0$ .

The work of Zhang and Lister [27, §5] on similarity solutions suggests that  $h(x, t) \sim \mathcal{B}^{1/4}(t_c - t)^{1/5} H(x/(t_c - t)^{2/5})$  as touchdown approaches; here  $t_c$  is the time of touchdown and  $H$  is a particular positive function with  $H(\eta) \sim (0.807)|\eta|^{1/2}$  for large  $\eta$ . Our computations are consistent with the above ansatz. Further, if we make the ansatz then we can estimate  $t_c$ , since taking the ratio of the computed values of  $h(0, t)$  at two late times  $t_1$  and  $t_2$  gives the value of  $(t_c - t_1)^{1/5}/(t_c - t_2)^{1/5}$ , from which  $t_c$  can be determined. We find  $t_c$  is slightly larger than the final resolved time. See [25, 26] for more on the similarity solutions to (8).

The most plausible future behavior for the solution in Figure 4 is that the solution might touch down in finite time and become a nonnegative weak solution. Then it might relax, as a weak solution, to a droplet steady state. Alternatively, since the energy of the original periodic steady state is higher than the energy of the constant steady state, the solution might perhaps touch down in finite time and then at some later time become positive and smooth again, ultimately relaxing to the constant steady state. This is certainly possible since the solution shown in the right of Figure 4 has higher energy than the constant steady state. However, we did not write our code to study finite-time singularities or weak solutions, and consequently we cannot distinguish which (if any) of the above options might be happening.

We close with a graphic demonstration of the kind of spurious effects that can occur if the solution is *not* spectrally resolved. In the left plot of Figure 5 we present the 8192 meshpoint solution that starts from the same initial data as in Figure 4. The right plot of Figure 5 shows the corresponding power spectra: as the solution evolves, higher and higher frequencies are needed to resolve the ever-sharpening local minimum, until at the final time resolution has

been lost. At this time the solution has multiple oscillations. We found those oscillations then grew and the solution seemed to touch down in finite time with two droplets per period, one large and one small. But the small droplet is a numerical artifact, in view of the absence of small droplets in the resolved solution shown in Figure 4.

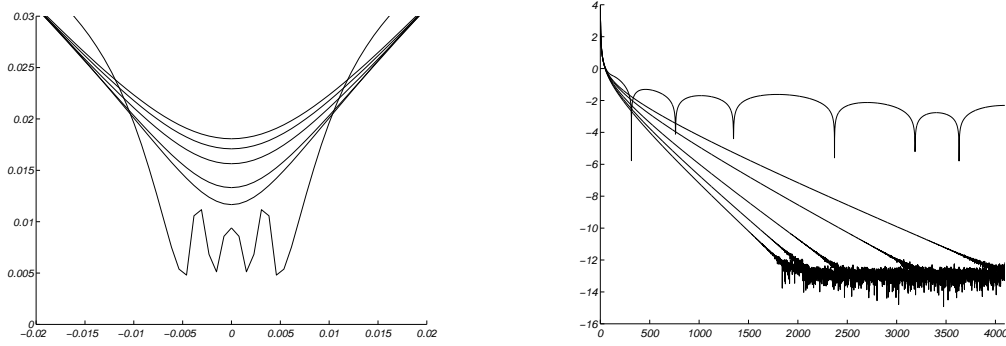


Fig.5: Left: evolution near  $x = 0$  of the solution with 8192 meshpoints. Right: the corresponding power spectra. The power spectrum reaches the Nyquist frequency soon after  $t = .04716$ , and the solution loses resolution. The profile on the left with multiple local minima is after  $t = .04716$ . The profiles with a single local minimum are spectrally resolved.

- *Odd perturbations.*

We now turn to odd perturbations. An obvious choice is the perturbation  $\varepsilon h'_{\text{ss}}$ ; it arises naturally from a leftwards translation of  $h_{\text{ss}}$ , since  $h_{\text{ss}}(x + \varepsilon) \approx h_{\text{ss}}(x) + \varepsilon h'_{\text{ss}}(x)$ . This perturbation shifts the local minimum of the initial data from  $x = 0$  to a point slightly to the left of  $x = 0$ , and it also lowers the minimum value since for small  $x < 0$ ,

$$h_{\text{ss}}(x) + \varepsilon h'_{\text{ss}}(x) = h_{\text{ss}}(0) + \varepsilon h''_{\text{ss}}(0)x + O(x^2) < h_{\text{ss}}(0).$$

Given initial data  $h_{\text{ss}} + 10^{-4}h'_{\text{ss}}$ , we expect the solution either to approach zero at some point or to relax to the constant steady state, since  $h_{\text{ss}}$  is energy unstable in the direction  $\pm h'_{\text{ss}}$  by [19, Theorem 2]. The simulation confirms this expectation, yielding a solution that touches down in a fashion very similar to the solution shown in Figure 4. One difference is that the location of the local minimum is no longer fixed in space; it moves as  $h_{\text{min}}(t) \rightarrow 0$ . The similarities are that the minimum value of the initial data is very close to zero, relative to the bulk of the initial data, and that the local minimum of the solution appears to decrease to zero in finite time while the bulk of the solution is essentially unchanged from the initial data.

- *Random perturbations.*

The equation (8) is translation invariant so there is nothing to distinguish any particular point in space. Up until now, we used either even or odd perturbations, making  $x = 0$  appear somewhat distinguished. To check the degree to which the behaviors described above depend on the choice of perturbation, we performed a number of runs with random perturbations.

The random perturbations are constructed as follows. The 2048 meshpoints can resolve 1023 frequencies, so we chose  $\{a_k\}$  and  $\{\phi_k\}$  to be two sets of 1023 uniformly distributed

random numbers in  $[0, 1]$  and defined the perturbation

$$\phi(x) = \sum_{k=1}^{1023} a_k \exp(-.036k) \cos(kx + 2\pi\phi_k).$$

This perturbation has zero mean, and has random amplitudes and phases at each wave-number. The decay rate 0.036 is chosen so that the amplitudes at wave numbers  $k = 900$  and higher are at the level of round-off error, so that the initial data is spectrally resolved. We then divided  $\phi$  by its  $L^\infty$  norm.

We found that all the solutions resulting from applying such a random perturbation to  $h_{\text{ss}}$  either relaxed to the constant steady state or else appeared to touch down in finite time. An intuitive rule might be that if the minimum value of the initial data is greater than that of  $h_{\text{ss}}$  then the solution should relax to the constant steady state and if the minimum value is less than that of  $h_{\text{ss}}$  then the solution should touch down in finite time. In practice, we found that most solutions respected this intuition, and the solutions that appeared to touch down in finite time had their gross dynamics as described earlier (their finer dynamics concern the position of the local minimum as a function of time). However, there were exceptions — hardly surprising since the evolution equation is a fourth order PDE, not second order, and the intuitive rule has the flavor of a comparison principle.

4.1.2.  $q = -3$ . *Perturbing the constant steady state.* Consider the constant steady state  $h \equiv \bar{h}$ , for some Bond number  $\mathcal{B}$ . If  $\mathcal{B}\bar{h}^{q-1} < 1$  then  $\bar{h}$  is a strict local minimum of the energy by [19, Theorem 10], and is nonlinearly stable. In this case a non-constant positive periodic steady state  $h_{\text{ss}}$  exists with period  $2\pi$  and mean value  $\bar{h}$  by [18, Theorem 12], since  $0 < \mathcal{B}\bar{h}^{q-1}(2\pi)^2 < (2\pi)^2$ ; it is linearly unstable (see bifurcation diagram 2a). If  $\mathcal{B}\bar{h}^{q-1} > 1$  then the constant steady state  $\bar{h}$  is a saddle point for the energy and we expect it to be unstable. In this case there is no stable positive periodic steady state to which a perturbation could converge (see bifurcation diagram 2a), suggesting that the solution will touch down in finite or infinite time.

- *Cosine perturbations.*

We take  $\mathcal{B} = 1$ . Consider the constant steady state  $\bar{h} = 2$ , a local minimum of the energy since  $\mathcal{B}\bar{h}^{q-1} < 1$ . Here the constant steady state is linearly stable and there exists a linearly unstable positive periodic steady state, by above. Given initial data  $2 - 10^{-4} \cos x$ , the solution appears numerically to relax to the constant steady state.

On the other hand, the constant steady state  $\bar{h} \equiv 1/2$  is linearly unstable and is a saddle point of the energy. Indeed, for initial data  $1/2 - 10^{-4} \cos x$  we find a solution that appears to touch down in finite time. Figure 6 shows this evolution over two periods. The top plot shows the short-time dynamics: the local minimum decreases, while the local maximum increases for a while. The top then “flattens” and two local maxima form one to each side

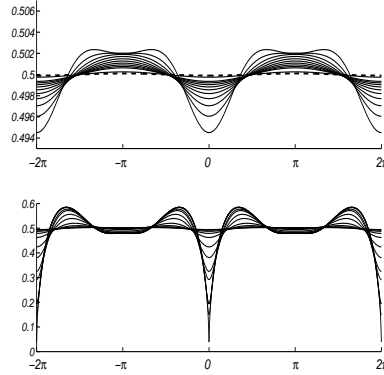


Fig.6:  $q = -3, n = 3$ . Dashed: initial data  $1/2 - 10^{-4} \cos(x)$ . The local minimum is at  $x = 0$  at all times and decreases monotonically to zero.

of the flat region. The bottom plot shows the later-time dynamics: the solution appears to touch down at one point per period and continues to have two local maxima per period. The final profile presented does not look like any known steady state, and so we expect the solution to continue evolving after touching down.

- *Random perturbations.*

Using random perturbations, we verified that the above results are robust: the steady state  $\bar{h} = 2$  is asymptotically stable and  $\bar{h} = 1/2$  is unstable.

Incidentally, we verified that the evolution is exponential in time near the periodic and constant steady states. This is consistent with the nonlinear behavior being dominated by the linear theory when the solution is sufficiently near a steady state. We found there was a short transient before the exponential behavior began, suggesting that the direction  $h''_{ss}$  is near but not equal to the first eigendirection. During the transient time, the solution is locating this eigendirection.

#### 4.2. $q = 0.5$ .

*Characteristic features of  $q \in (-1, 1)$ : positive periodic steady states are linearly unstable. A ‘Mountain pass’ scenario can occur — the energy of the non-constant positive periodic steady state is higher than the energies of the constant steady state and a zero-contact angle droplet steady state. (See bifurcation diagram 2b and remarks after [19, Theorem 11].)*

We take  $n = 1, m = .5, q = 0.5$  and compute solutions of

$$h_t = -(h^1 h_{xxx})_x - \mathcal{B}(h^{.5} h_x)_x.$$

4.2.1.  $q = 0.5$ , *perturbing the positive periodic steady state.* We rescale a steady state  $k_\alpha$  with minimum height  $\alpha = 0.03000$  and period  $P(\alpha) = 6.049$ . This yields a Bond number  $\mathcal{B} = 0.9628$  and positive periodic steady state  $h_{ss}$  with period  $2\pi$  and area  $A_{ss} = 7.980$ . Note  $h_{ss}$  is linearly unstable, by bifurcation diagram 2b with  $\mathcal{B}P_{ss}^{3-q}A_{ss}^{q-1} = 35.59$ .

- *Even perturbations.*

As in §4.1.1, we perturb  $h_{ss}$  with  $\pm 10^{-4}h''_{ss}$ .

For the initial data  $h_{ss} + 10^{-4}h''_{ss}$ , we expect to see evidence of a heteroclinic connection to the constant steady state  $\overline{h_{ss}}$ , for the same reasons given for the  $q = -3$  case, and indeed our simulation turned out to be very similar to that shown in Figure 3.

Next, for the initial data  $h_{ss} - 10^{-4}h''_{ss}$  we find the solution appears to touch down in finite time. Like the  $q = -3$  simulation,  $h_{min}(t)$  is located at  $x = 0$  and, except for a short transient, decreases monotonically in time. Figure 7a presents  $h$  at the final resolved time.

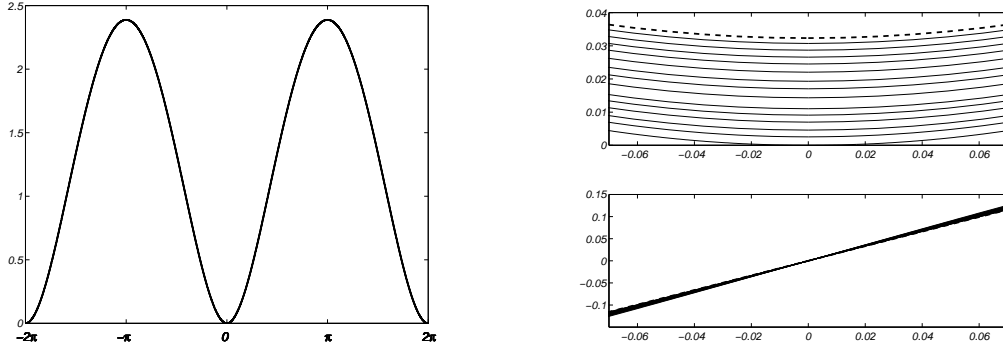


Fig.7:  $q = .5$ ,  $n = 1$ . Left:  $h$  at final resolved time,  $t = 7.762540625$ , shown over two periods with 8192 meshpoints per period. Right top: close-up of  $h$  near pinch-off; minimum decreases monotonically after a short transient; dashed line is initial data. Right bottom: close-up of  $h_x$  at same times.

Since  $-1 < q < 1$ , [19, Theorem 7] tells us there exists a zero-angle droplet steady state  $\hat{h}_{ss}$  that has the same area as  $h_{ss}$ , has length less than  $2\pi$ , and has lower energy than  $h_{ss}$ . And indeed Figure 7a shows a profile that appears to be close to a zero-contact-angle solution. As further evidence of this, in the top plot of Figure 7b we present a close-up of the evolution near the touch-down point. In the bottom plot we present  $h_x$  at those times: the slope does not appear to be forming a jump discontinuity, which it would have to be doing were the solution converging to a solution with nonzero contact angle.

- *Odd perturbations.*

The odd perturbation  $10^{-4}h'_{ss}$  yields an evolution qualitatively like that of  $q = -3$  above. The solution appears to touch down in finite time, with the late-time behavior much like that shown in the right top plot of Figure 7.

- *Random perturbations.*

For random perturbations, we observed the same type of dynamics as seen in the  $q = -3$  case. Some perturbations led to solutions that relaxed to the constant steady state, and others yielded solutions that appeared to touch down in finite time with a late-time evolution like in the right top plot of Figure 7.

*Mountain pass:* Our simulations above numerically confirm for  $q = .5$  the following ‘mountain pass’ scenario, which is possible whenever  $-1 < q < 1$ .

Choose a positive periodic steady state  $h_{\text{ss}}$  such that  $\mathcal{B}(2\pi)^{3-q}A_{\text{ss}}^{q-1}$  lies between  $E_0(q)$  and  $4\pi^2$  (see [19, Figure 6] and refer to the existence result [18, Theorem 12]). This positive periodic steady state is linearly unstable and has higher energy than the constant steady state  $h \equiv \overline{h_{\text{ss}}}$ , by [18, Theorem 7] and [19, Theorem 6]. It also has higher energy than the zero-angle droplet steady state  $\hat{h}_{\text{ss}}$  by [19, Theorem 7]. Further, the constant steady state  $\overline{h_{\text{ss}}}$  is linearly stable and is a local minimum of the energy, by [19, Theorem 10].

Thus the positive periodic steady state  $h_{\text{ss}}$  appears to sit at a ‘mountain pass’ between the constant steady state  $\overline{h_{\text{ss}}}$  (which lies at the bottom of an energy well) and the droplet state  $\hat{h}_{\text{ss}}$ . If in addition  $\mathcal{B}(2\pi)^{3-q}A_{\text{ss}}^{q-1} > L(q)$  (see [19, Figure 6] for  $L(q)$ ) then the constant steady state has higher energy than the droplet, by [19, Theorem 11]. But regardless of that, one would expect that perturbing  $h_{\text{ss}}$  in one direction would lead to a solution that converges to the constant steady state while perturbing in the other direction would lead to a single droplet. Our numerics for  $q = .5$  are all consistent with this expectation.

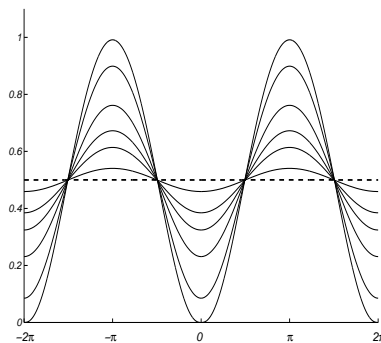


Fig.8:  $q = .5, n = 1$ . Dashed: initial data  $1/2 - .0001 \cos x$ . The local minimum and maximum are fixed in space and, after a short transient, decrease (increase) monotonically.

4.2.2.  $q = 0.5$ , *perturbing the constant steady state*. As in the  $q = -3$  case, we take  $\mathcal{B} = 1$  and consider perturbing the constant steady states  $h \equiv 2$  ( $\mathcal{B}\overline{h}^{q-1} < 1$ ) and  $h \equiv 1/2$  ( $\mathcal{B}\overline{h}^{q-1} > 1$ ). The first steady state is linearly stable while the second is linearly unstable. We perturbed the two states with a range of perturbations, and found that all perturbations of  $h \equiv 2$  relaxed to  $h \equiv 2$ , while all perturbations of  $h \equiv 1/2$  led to apparent finite-time touch-down.

In Figure 8, for example, we plot the evolution of the solution with initial data  $1/2 - .0001 \cos(x)$ . The extrema are located at  $x = 0$  and  $2\pi$  and, after a short transient, increase (decrease) monotonically. The evolution shown here is very standard; we observed this type of behavior more often than the type shown in Figure 6

#### 4.3. $q = 1$ .

*Characteristic features for  $q = 1$ : all positive periodic steady states are linearly neutrally stable.* (See bifurcation diagram 2c and [19, Lemma 4].)

Here we consider the  $q = 1$  case, for which the non-constant positive periodic steady states are neutrally stable. We take  $n = m = 1$  and compute solutions of

$$h_t = -(h^1 h_{xxx})_x - \mathcal{B}(h^1 h_x)_x.$$

Goldstein et al. [13, Fig. 3a] found that fairly large multi-modal perturbations of such steady states relax to steady states. They found the solution may relax to a different steady state than the one of which it was initially a perturbation.

For  $\mathcal{B} = 2(1 - \cos(\Delta x))/(\Delta x)^2 = 1 - O(\Delta x^2)$ , one finds a finite-difference steady state by sampling  $a + b \cos(x) + c \sin(x)$  on a  $\Delta x$ -uniform mesh (see §6.3). In the left plot of Figure 9, we present two simulations confirming that each positive periodic steady state is nonlinearly stable and that a small perturbation of a positive periodic steady state converges to a (potentially different) positive periodic steady state. In the top left plot, we present the evolution from initial data  $1 - .8 \cos(x) + .3v(x)$  where  $v$  is a zero-mean random perturbation. In the bottom left plot, we present the evolution from initial data  $1 - .8 \cos(x) - .19 \exp(-100 \sin^2(x/2)) + .19 \exp(-100 \sin^2((x - \pi)/2))$ . In both cases, the solution relaxes to a positive periodic steady state with an amplitude close to .8 and a local minimum close to  $x = 0$ . We find that the smaller the perturbation, the closer the long-time limit is to the original steady state, numerically demonstrating nonlinear stability. We have no rule for predicting the amplitude of the long-time limit and, unless the perturbation is even, we have no way of predicting the position of the local minimum.

Since these simulations suggest that the non-constant positive periodic steady states are nonlinearly stable, one might guess that one cannot find a solution that touches down in finite time. This is certainly what we observed for  $q = 1.5$  and  $q = 1.768$  in §4.4–4.5. And as the bottom left plot of Figure 9 suggests, initial data that has a sharp local minimum will likely not evolve towards touch-down; the local minimum will retract in time, as expected for a solution of a surface-tension driven flow. But initial data that is very flat near its local minimum, such as  $h_0(x) = .7 - .8 \cos(x) + .19 \cos(2x)$ , does appear to lead to touch-down in finite time, as shown in the top right plot of Figure 9. The bottom right plot shows the local evolution near the touch-down point.

The  $q = 1$  case remains mysterious in many ways, because there are infinitely many  $2\pi$ -periodic steady states all having the same mean value; in the  $q \neq 1$  case there are at most two.

*Note:* numerical simulations for  $q = 1$  were earlier presented with  $m = n = 1$  in [13], with  $m = n = 2$  in [15, §8], and with  $m = n = 3$  in [8]. The latter two articles do not consider Bond numbers for which periodic steady states might be observed.

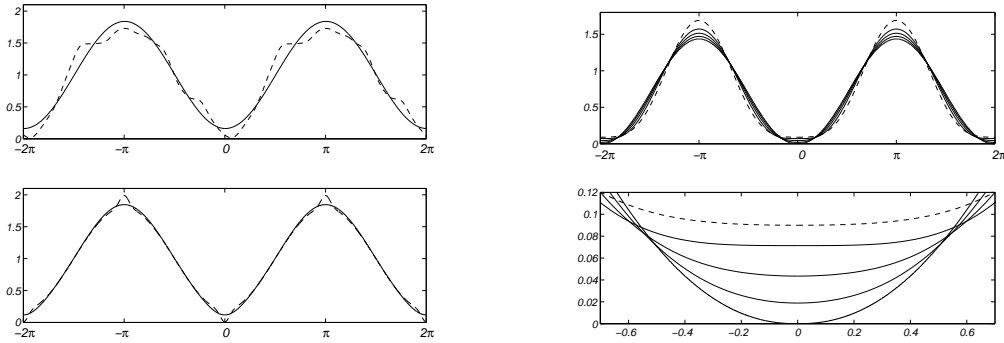


Fig.9:  $q = 1$ ,  $n = 1$ ; dashed line: initial data. Top left:  $h_0(x) = 1 - .8 \cos(x) + .3v(x)$  where  $v$  is a random perturbation. Bottom left:  $h_0(x) = 1 - .8 \cos(x) - .19 \exp(-100 \sin^2(x/2)) + .19 \exp(-100 \sin^2((x - \pi)/2))$ . In both cases, solution relaxes to a steady state. Right:  $h_0(x) = .7 - .8 \cos(x) + .19 \cos(2x)$  with minimum value .09. Extrema are fixed in space and change monotonically (after a short transient), with  $h_{min}(t)$  touching down in finite time. The final resolved solution is on 32,768 meshpoints with  $h_{min} = 1.02 \cdot 10^{-7}$ .

#### 4.4. $q = 1.5$ .

*Characteristic features for  $q \in (1, 1.75]$ : positive periodic steady states are linearly stable.* (See bifurcation diagrams 2d–e.)

We take  $n = 1$ ,  $m = 1.5$ ,  $q = 1.5$ , and compute solutions of

$$h_t = -(h^1 h_{xxx})_x - \mathcal{B}(h^{1.5} h_x)_x.$$

4.4.1.  $q = 1.5$ . *Perturbing the positive periodic steady state.* We rescale a steady state  $k_\alpha$  with minimum height  $\alpha = 0.2145$ , period  $P_\alpha = 6.453$ . With  $D = 1$  this yields a Bond number  $\mathcal{B} = 1.083$  and positive periodic steady state  $h_{ss}$  with period  $P_{ss} = 2\pi$  and area  $A_{ss} = 5.516$ , and with minimum at  $x = 0$ . This positive periodic steady state is linearly stable, unlike for the other  $q$ -values considered so far; see bifurcation diagram 2d with  $\mathcal{B}P_{ss}^{3-q}A_{ss}^{q-1} = 40.07$ .

- *Even perturbations.*

We perturb  $h_{ss}$  with  $\pm 10^{-4} h''_{ss}$ , and expect to see the solution relax back to  $h_{ss}$ , since  $h_{ss}$  is linearly stable and since translation in space is ruled out by the evenness of  $h_{ss}$  and of our perturbation. Numerically, we indeed observe relaxation back to  $h_{ss}$ : the extrema are at  $x = 0$  and  $\pi$  and, after a short transient, they move monotonically to the maximum and minimum values of  $h_{ss}$ .

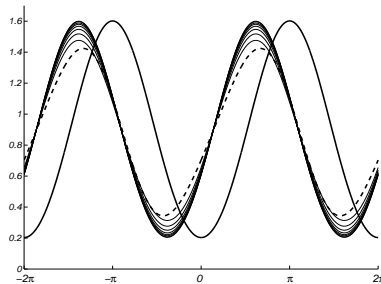


Fig.10:  $q = 1.5$ ,  $n = 1$ . Dashed line: initial data  $h_{ss} + .5h'_{ss}$ . Isolated solid line:  $h_{ss}$ . Solution relaxes to a translate of  $h_{ss}$ ; extrema move in time.

- *Odd perturbations.*

We now perturb  $h_{\text{ss}}$  with  $.5h'_{\text{ss}}$ , which is a large perturbation relative to those discussed above. In view of the linear stability and the fact that every perturbation increases the energy, by [19, Theorem 5], we expect to observe relaxation back to a translate of  $h_{\text{ss}}$ . (Note the energy and our linear stability results are insensitive to translation.) Convergence back to  $h_{\text{ss}}$  itself (with no translation) seems unlikely since the odd perturbation breaks the evenness of the initial data.

Figure 10 displays the evolution of the solution with initial data  $h_{\text{ss}} + .5h'_{\text{ss}}$ ; the solution certainly seems to converge to a translate of  $h_{\text{ss}}$ . We verified this type of behavior for a range of  $q \in (1, 1.75]$ .

- *Random perturbations.*

Using random perturbations, we verified the robustness of the above results: the periodic steady state  $h_{\text{ss}}$  is asymptotically stable, up to translation.

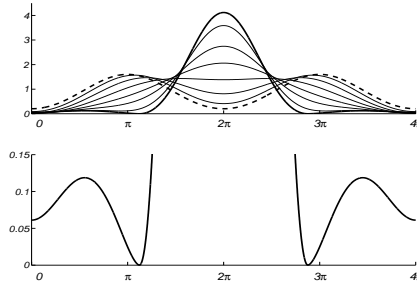


Fig.11:  $q = 1.5$ ,  $n = 1$ . Top plot: dashed line is initial data  $h_{\text{ss}} - .0001 \cos(x/2)$ ; heavy solid line is final resolved solution at  $t = 61.7305$ , with 4096 meshpoints. Bottom plot: close-up of final resolved solution.

4.4.2.  $q = 1.5$ . *Perturbing the positive periodic steady state with longer perturbations.* We have demonstrated above that the positive periodic steady state  $h_{\text{ss}}$  is asymptotically stable to small perturbations of the same period,  $2\pi$ . However, it is linearly *unstable* to zero-mean perturbations of *longer* period —  $4\pi$ ,  $6\pi$  and so on — by [18, Theorem 1].

For initial data  $h_{\text{ss}} - .0001 \cos(x/2)$ , *i.e.* a perturbation with period  $4\pi$ , the top plot of Figure 11 presents the evolution of the solution. The steady state  $h_{\text{ss}}$  has minimum heights at  $x = 0, 2\pi$ , while the perturbation  $-.0001 \cos(x/2)$  is even about  $x = 2\pi$  and decreases the initial value at  $x = 0$  and increases the value at  $x = 2\pi$ . The solution appears to touch down in finite time, though it does not do so at  $x = 0$ ; also the solution does not appear to be converging to a single droplet. The bottom plot of Figure 11 shows a close-up of the final resolved solution. The smaller droplet is not close to a steady droplet, since it contains a local minimum within itself — an impossibility for a steady droplet. We expect the solution would continue to evolve as a nonnegative weak solution, relaxing either to a single steady droplet or to some (unknown) configuration of steady droplets.

We also considered a number of *random*  $4\pi$ -periodic perturbations, and always found that the solution appears to touch down in finite time with one large droplet flanked as in Figure 11 by a smaller profile which contains a local minimum within itself.

4.4.3.  $q = 1.5$ . *Perturbing the constant steady state.* We take  $\mathcal{B} = 1$ . As always, the constant steady state  $h_{ss} \equiv \bar{h}$  is a strict local minimum of the energy if  $\mathcal{B}\bar{h}^{q-1} < 1$  (or  $\bar{h} < 1$ ), and is a saddle point if  $\mathcal{B}\bar{h}^{q-1} > 1$  (or  $\bar{h} > 1$ ).

- *Cosine perturbations.*

We consider  $\bar{h} = .5, 1.05$ , and  $2$ . We expect  $\bar{h} = .5$  will be stable to all perturbations, and that  $\bar{h} = 1.05$  and  $\bar{h} = 2$  will be unstable to some perturbations.

For  $\bar{h} = 1.05$ , there exists a linearly stable positive  $2\pi$ -periodic steady state with mean value  $1.05$ , by bifurcation diagram 2d, using that  $E := \mathcal{B}\bar{h}^{q-1}(2\pi)^2 \in (4\pi^2, E_0(q))$  when  $\mathcal{B} = 1, q = 1.5$  and  $\bar{h} = 1.05$ , since  $E_0(q) = 40.67$ . (See [17, §3.1.2] for the formula for  $E_0(q)$ .) A perturbation of  $\bar{h} = 1.05$  might converge to this positive periodic steady state, especially since:  $h_{ss}$  is linearly stable;  $h_{ss}$  should have lower energy than  $\bar{h}$ , as discussed after [19, Theorem 6]; and there is no zero-angle droplet steady state with length less than  $2\pi$  and the same area as  $\bar{h}$ , by [19, Theorem 8]. (Note: we cannot exclude that the solution might converge to a droplet steady state with nonzero contact angle.)

On the other hand, for  $\bar{h} = 2$  there is no positive steady state with least period  $2\pi$  and mean value  $2$ , since  $\mathcal{B}\bar{h}^{q-1}(2\pi)^2 \notin (4\pi^2, E_0(q))$ . (Or see bifurcation diagram 2d.) For this reason, we expect that perturbations of  $\bar{h} = 2$  should lead to solutions that converge to a configuration of steady droplets.

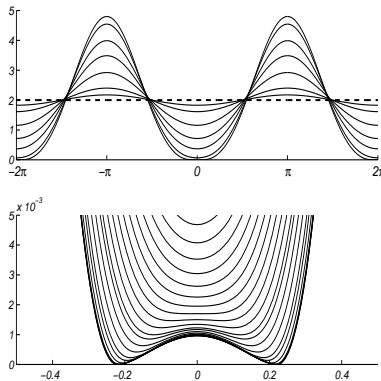


Fig.12:  $q = 1.5, n = 1$ . Dashed line:  $h_0(x) = 2 - .0001 \cos(x)$ . The maximum points are fixed; the minimum is initially at  $x = 0$  but then splits into two minima which move apart in time as they decrease.

We take initial data  $\bar{h} - 10^{-4} \cos x$ . We find that if  $\bar{h} = .5$  then the solution relaxes to the constant steady state and if  $\bar{h} = 1.05$  then the solution relaxes to the positive periodic steady state. In both cases, the dynamics are very natural, somewhat like Figure 3 (but run in reverse when  $\bar{h} = 1.05$ ), with the local extremum points fixed in space and the corresponding extremal values evolving monotonically in time, after a short transient. For

$\bar{h} = 2$ , the solution appears to be converging to a configuration with two droplets per period (see Figure 12). All the solutions shown in this figure are numerically resolved; the small droplet is real rather than a numerical artifact, although it may later vanish as the solution evolves.

- *Random perturbations.*

Random zero-mean perturbations led to solutions with the same dynamics: perturbations of  $\bar{h} = .5$  relaxed to the mean, perturbations of  $\bar{h} = 1.05$  relaxed to a translate of the positive periodic steady state  $h_{\text{ss}}$ , and perturbations of  $\bar{h} = 2$  appeared to converge to a configuration of two droplets.

#### 4.5. $\mathbf{q} = 1.768$ .

*Characteristic features for  $q \in (1.75, 1.79)$ : some positive periodic steady states are linearly stable, while others are linearly unstable; and there can be more than one positive periodic steady state with the same period and area.* (See bifurcation diagrams 2f–h, and [17, §5.1].)

We take  $n = 1$ ,  $m = 1.768$ ,  $q = 1.768$ , and compute solutions of

$$h_t = -(h^1 h_{xxx})_x - \mathcal{B}(h^{1.768} h_x)_x.$$

4.5.1.  $q = 1.768$ . *Perturbing the positive periodic steady states.* For  $q$ -values in the interval  $(1.75, 1.794]$  (approx.) a new possibility arises: a heteroclinic connection between two fundamentally different positive periodic steady states. We investigate this possibility in what follows.

For Bond number  $\mathcal{B} = 1.257$  we consider two distinct positive periodic steady states,  $h_{\text{ss}1}$  and  $h_{\text{ss}2}$ , that have least period  $2\pi$ , area  $A = 4.661$ , and have their local minima at  $x = 0$ . We denote the steady state that has lower minimum value by  $h_{\text{ss}1}$ , and the other by  $h_{\text{ss}2}$ . Then we expect  $h_{\text{ss}1}$  to be linearly stable and  $h_{\text{ss}2}$  to be unstable, by [19, Theorem 9] and its accompanying remarks, with  $h_{\text{ss}1}$  having lower energy. That is,  $h_{\text{ss}1}$  lies on the stable branch of the bifurcation diagram 2g and  $h_{\text{ss}2}$  lies on the unstable branch (since  $\mathcal{B}P_{\text{ss}}^{3-q}A_{\text{ss}}^{q-1} = 39.46$ .) Note also that the constant steady state  $h := \overline{h_{\text{ss}1}}$  is linearly stable since  $\mathcal{B}\bar{h}^{q-1} < 1$ .

We consider even perturbations ( $\varepsilon h''_{\text{ss}}$ ), odd perturbations ( $\varepsilon h'_{\text{ss}}$ ), and random perturbations. Our simulations show that  $h_{\text{ss}1}$  has stability properties like the  $q = 1.5$  steady state  $h_{\text{ss}}$  examined in §4.4. The other steady state  $h_{\text{ss}2}$  is unstable. For example, the initial data  $h_{\text{ss}2} + 10^{-4}h''_{\text{ss}2}$  yields a solution that converges to the constant steady state, as shown in Figure 13(a). The initial data  $h_{\text{ss}2} - 10^{-4}h''_{\text{ss}2}$  yields a solution converging to  $h_{\text{ss}1}$  as  $t \rightarrow \infty$ , as shown in Figure 13(b). The observed behavior is very robust, and strongly suggests existence of a heteroclinic connection from the unstable steady state  $h_{\text{ss}2}$  to the stable one  $h_{\text{ss}1}$ .

Perturbing  $h_{\text{ss}2}$  with *random* zero-mean perturbations yields evidence of heteroclinic connections from  $h_{\text{ss}2}$  to *translates* of  $h_{\text{ss}1}$  and to the constant steady state.

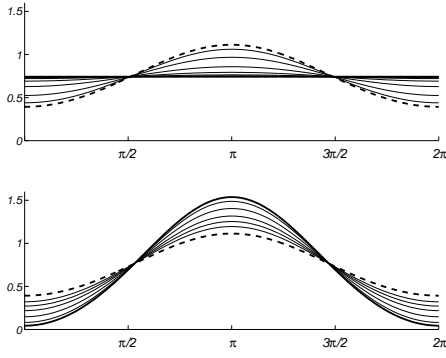


Fig.13:  $q = 1.768$  and  $n = 1$ . (a) Dashed:  $h_{ss2} + 10^{-4}h''_{ss2}$ ; solid:  $\overline{h_{ss2}}$ . Solution relaxes to constant. (b) Dashed:  $h_{ss2} - 10^{-4}h''_{ss2}$ ; solid:  $h_{ss1}$ . Solution relaxes to  $h_{ss1}$ .

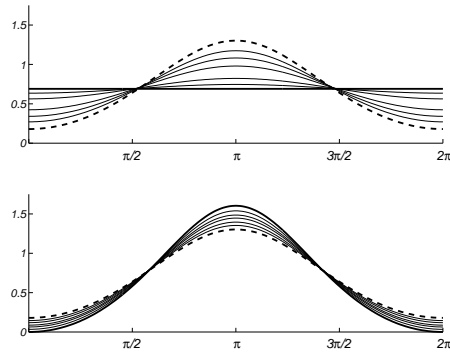


Fig.14:  $q = 2.5$  and  $n = 1$ . (a) Dashed:  $h_{ss} + 10^{-4}h''_{ss}$ ; solid:  $\overline{h_{ss}}$ . Solution relaxes to  $\overline{h_{ss}}$ . (b) Dashed:  $h_{ss} - 10^{-4}h''_{ss}$ . Solution touches down in finite time.

We now explain how we found the two steady states  $h_{ss1}$  and  $h_{ss2}$  having the same period and area, since this is not completely obvious. First we plot  $E(\alpha)$  for  $\alpha \in (0, 1)$ , as in [19, Figure 5]. We seek  $\alpha_1 < \alpha_2$  such that  $E(\alpha_1) = E(\alpha_2)$  with  $E'(\alpha_1) < 0$  and  $E'(\alpha_2) > 0$ . Choosing  $\alpha_1 = .05$ , it is graphically clear from [19, Figure 5] that the desired  $\alpha_2$  exists. To determine it, we compute  $k_{\alpha_1}$  and its period  $P(\alpha_1) = 6.703$  and area  $A(\alpha_1) = 5.660$ , and hence  $E(\alpha_1) = 39.46$ . Taking  $\alpha = \alpha_1$  and  $D = D_1 = 1$  and  $P_{ss} = 2\pi$  in the rescaling relations [19, eq. (24)] we evaluate the Bond number as  $\mathcal{B} = 1.257$ . We then find six values of  $\alpha$  such that  $E(\alpha) < E(\alpha_1)$  at the first three values and  $E(\alpha) > E(\alpha_1)$  at the last three values, so that  $\alpha_2$  is between the third and fourth values. We interpolate  $E$  at these six values of  $\alpha$  with a quintic polynomial and use Newton–Raphson iteration to find  $\alpha_2 = 0.5069$  satisfying  $E(\alpha_1) = E(\alpha_2)$ . We find  $k_{\alpha_2}$  has period  $P(\alpha_2) = 6.388$  and area  $A(\alpha_2) = 6.115$ . Then  $P(\alpha_2)$  and the Bond number  $\mathcal{B}$  determine the integration constant  $D_2 = 0.8010$  from [19, eq. (24)], using again  $P_{ss} = 2\pi$ . Using  $D_1$  and  $\mathcal{B}$  and [19, eq. (7)], we rescale  $k_{\alpha_1}$  to find  $h_{ss1}$ ; by similarly using  $D_2$  we rescale  $k_{\alpha_2}$  to find  $h_{ss2}$ . Then we use  $h_{ss1}$  and  $h_{ss2}$  to determine finite difference steady states, as in §6.3.

#### 4.6. $q = 2.5$ .

*Characteristic features of  $q \in (1.8, 3)$ : positive periodic steady states are linearly unstable. ‘Mountain pass’ scenario can occur.* (See bifurcation diagram 2i and remarks after [19, Theorem 11].)

We take  $n = 1$ ,  $m = 2.5$ ,  $q = 2.5$  and compute solutions of

$$h_t = -(h^1 h_{xxx})_x - \mathcal{B}(h^{2.5} h_x)_x.$$

4.6.1.  $q = 2.5$ . *Perturbing the positive periodic steady state.* For Bond number  $\mathcal{B} = 1.561$  we consider a positive periodic steady state  $h_{ss}$  with period  $2\pi$  and area  $A_{ss} = 4.335$ . This arises from rescaling  $k_\alpha$  with minimum height  $\alpha = 0.2145$  and period  $P_\alpha = 6.869$ . Here  $h_{ss}$  is linearly unstable.

Figure 14(a) presents the solution with initial data  $h_{\text{ss}} + 10^{-4}h''_{\text{ss}}$ , which converges to the constant steady state as time passes. Figure 14(b) shows the solution with initial data  $h_{\text{ss}} - 10^{-4}h''_{\text{ss}}$ , which appears to touch down in finite time. These numerical results are qualitatively the same as for  $q = 0.5$ , in §4.2. We found this behavior was very robust — we considered random perturbations (see §4.1.1) and found for each one that the solutions would either converge to the constant steady state or else touch down in finite time.

4.6.2.  $q = 2.5$ . *Perturbing the constant steady state.* Just as in the  $q = -3$  case, our numerics robustly confirm our predictions: for  $\mathcal{B}\bar{h}^{q-1} < 1$ , small zero-mean perturbations of  $\bar{h}$  yield solutions that relax to the constant steady state, while for  $\mathcal{B}\bar{h}^{q-1} > 1$  such perturbations yield solutions that appear to touch down in finite time.

#### 4.7. $q = 4$ .

*Characteristic features of  $q \in [3, \infty)$ : positive periodic steady states are linearly unstable, and if a positive periodic steady state and a zero-angle droplet steady state have the same area, then the period of the former is less than the length of the latter. (See [18, Theorem 7] and the proof of [19, Theorem 7].)*

We take  $n = 1$ ,  $m = 4$ ,  $q = 4$  and compute solutions of

$$(9) \quad h_t = -(h^1 h_{xxx})_x - \mathcal{B}(h^4 h_x)_x.$$

This equation is ‘super-critical’ in the sense of Bertozzi and Pugh [8], since  $m > n + 2$  (*i.e.*  $q > 3$ ). According to the conjecture in [8], then, positive periodic solutions can blow up in finite time ( $\|h(\cdot, t)\|_\infty \rightarrow \infty$ ). Bertozzi and Pugh made the same conjecture for compactly supported weak solutions on the line, and proved blow-up can occur in finite time when  $n = 1$  and  $m \geq n + 2 = 3$  [9]. Specifically, they proved for such cases that if the compactly supported initial data  $h_0(x)$  has negative energy

$$\mathcal{E}(h_0) = \int \left[ \frac{1}{2} h_0'(x)^2 - \frac{\mathcal{B}}{q(q+1)} h_0(x)^{q+1} \right] dx < 0,$$

then the compactly supported weak solution blows up in finite time, with its  $L^\infty$  and  $H^1$  norms both going to infinity.

Here we present computational evidence that smooth *periodic* solutions of (9) can also blow up in finite time (there is no proof of this). Further, we find initial data that has positive energy yet still appears to yield finite-time blow-up, suggesting that negativity of the energy is not necessary for blow-up, in the periodic case.

4.7.1.  $q = 4$ , *perturbing the positive periodic steady state.* For Bond number  $\mathcal{B} = 4.281$  we consider a positive periodic steady state  $h_{\text{ss}}$  with period  $2\pi$  and area  $A_{\text{ss}} = 3.213$ . This arises from rescaling  $k_\alpha$  with minimum height  $\alpha = 0.2145$  and period  $P_\alpha = 7.536$ . Here  $h_{\text{ss}}$  is linearly unstable and the energy  $\mathcal{E}(h_0) = .01445$  is positive.

- *Even perturbations.*

We considered initial data  $h_{ss} \pm .001h''_{ss}$ . The initial data  $h_{ss} + .001h''_{ss}$  yielded a solution that relaxed to the constant solution as time evolved. The local extrema were fixed in space and, after a short transient, relaxed monotonically to the mean.

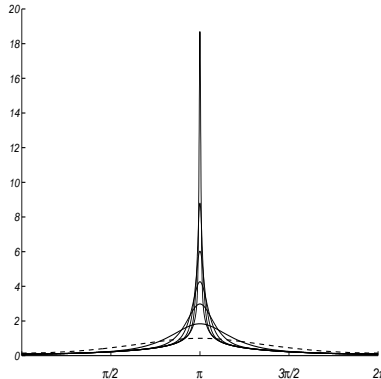


Fig.15:  $q = 4, n = 1$ . Dashed: initial data  $h_{ss} - .001h''_{ss}$ . In the figure, the maximum increases with time. The final profile, at  $t = 10.0282848199749$ , has 4096 meshpoints.

The initial data  $h_{ss} - .001h''_{ss}$  yielded a solution that appears to blow up in finite time (see Figure 15). The extrema are fixed in space and, after a short transient,  $h_{max}$  increases monotonically towards infinity (the figure shows  $h_{max}$  increasing by a factor of 18.7). After a short transient,  $h_{min}$  decreases monotonically to a positive value as the singular time approaches.

A self-similarity ansatz similar to the case  $q = -3$  suggests that  $h(x, t) \sim (t_c - t)^{-1/7} H((x - \pi)/(t_c - t)^{3/14})$  as blowup approaches at  $x = \pi$ ; here  $t_c$  is the time of blowup and  $H$  is a positive function with  $H(\eta) \sim C|\eta|^{-2/3}$  for large  $\eta$ . Our computations are consistent with the above ansatz. Again, if we make the ansatz then we can estimate the blowup time  $t_c$ , since taking the ratio of the computed values of  $h(\pi, t)$  at two late times  $t_1$  and  $t_2$  gives the value of  $(t_c - t_1)^{-1/7}/(t_c - t_2)^{-1/7}$ , from which  $t_c$  can be determined. We find that  $t_c$  is slightly larger than the final resolved time.

Self-similar blow-up for super-critical exponents has also been found for  $h_t = -(h^3 h_{xxx})_x - \mathcal{B}(h^6 h_x)_x$  in [10].

- *Odd perturbations.*

The odd perturbation  $10^{-3}h'_{ss}$  yielded an evolution qualitatively like that shown in Figure 15. The solution appears to blow up in finite time, with the location of the maximum moving in time.

- *Random perturbations.*

Random perturbations led to the same type of dynamics as seen with  $\pm h''_{ss}$  perturbations.

4.7.2.  $q = 4$ , *perturbing the constant steady state.* Our numerics robustly confirm our predictions: for  $\mathcal{B}\bar{h}^{q-1} < 1$ , small zero-mean perturbations of  $\bar{h}$  yield solutions that relax to the

constant steady state, while for  $\mathcal{B}\bar{h}^{q-1} > 1$  such perturbations yield solutions that appear to blow up in finite time.

## 5. THE EFFECT OF CHANGING THE MOBILITY EXPONENTS, $\mathbf{n}$ AND $\mathbf{m}$

In this section, we vary  $n$  and  $m$  in the equation  $h_t = -(h^n h_{xxx})_x - \mathcal{B}(h^m h_x)_x$ . We think of these exponents as *mobility* parameters, since they determine the diffusion coefficients of the fourth and second order terms in the equation. When we change  $n$  and  $m$ , we keep  $q = m - n + 1$  fixed, which means the steady states of the evolution are unchanged by §2. This allows us to ask three natural questions about the effects of changing the mobility exponents:

1. Can a heteroclinic orbit between steady states be *broken*, or is it merely perturbed?
2. Can the *type* of a singularity be altered (*e.g.* from finite-time to infinite-time)?
3. Can the *number* of singularities be altered (*e.g.* from one to two per period)?

The next three subsections address these questions.

Note that while one often thinks of the initial and terminal points of a heteroclinic connection as being *isolated* equilibrium points, here our equilibria are not isolated, for two reasons. First, the translates of a steady state are themselves all steady states with the same area. (Of course this translational freedom disappears when considering even perturbations of even initial data.) And second, when we consider configurations of droplet (compactly supported) steady states that consist of several droplets, the droplets can be translated, shrunk or expanded, subject only to the requirements that the total area (volume) be fixed and that the droplets remain disjoint.

**5.1. Perturbing heteroclinic orbits.** For  $q = 2.5$ , we computed a  $2\pi$ -periodic steady state  $h_{ss}$  with Bond number  $\mathcal{B} = 1.561$  and area 4.335, by rescaling  $k_\alpha$  with  $\alpha = 0.2145$  and  $P_\alpha = 6.869$ . The steady state is linearly unstable (see bifurcation diagram 2i with  $\mathcal{B}P_{ss}^{3-q}A_{ss}^{q-1} = 35.32$ .) We take initial data  $h_{ss} + .001h''_{ss}$ ; we expect to find solutions that relax to the constant steady state,  $\overline{h_{ss}} \equiv 0.6899$ . We vary the mobility exponents, by taking  $n = 0, 1, 2$ , and  $3$  in turn, and determining  $m$  from  $q = 2.5 = m - n + 1$ . That is, we compute solutions for the four evolution equations, all with the same initial data.

We find that all four solutions relax to the constant steady state; the apparent heteroclinic orbit is robust under this change in mobility. In the top left plot of Figure 16, we plot  $h_{min}$  and  $h_{max}$  versus time for the four solutions. The larger the exponent  $n$ , the longer it takes for the solution to relax to the constant steady state.

Since  $\overline{h_{ss}} < 1$ ,  $h_{min}(t) < 1$  for all time and there is a time  $t_1$ , dependent on  $n$ , such that  $h_{max}(t) > 1$  for  $t < t_1$  and  $h_{max}(t) < 1$  for  $t > t_1$ . Near the minimum point,  $h^0 > h^1 > h^2 > h^3$ , suggesting that the larger  $n$  is, the slower the diffusion will be (near the

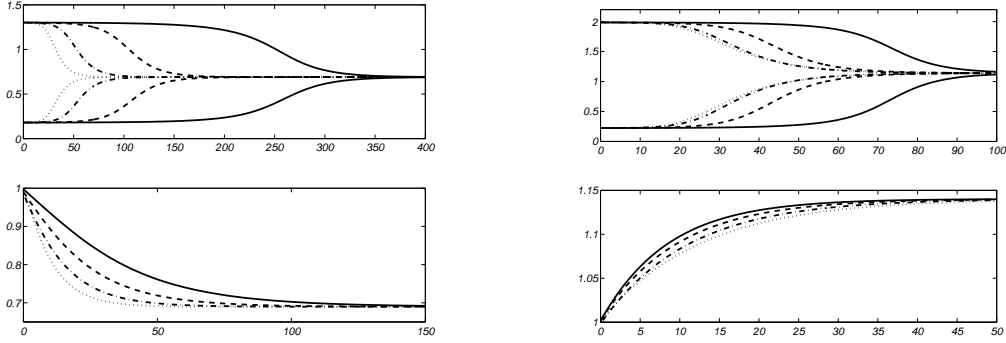


Fig.16: Dotted  $n = 0$ , dot-dashed  $n = 1$ , dashed  $n = 2$ , solid  $n = 3$ . Left:  $q = 2.5$ . Top left:  $h_{max}(t)$  and  $h_{min}(t)$  versus  $t$ . Bottom left:  $h_{max}(t - t_1)$  versus  $t - t_1$ , where  $h_{max}(t_1) = 1$ . Right:  $q = 0.5$ . Top right:  $h_{max}(t)$  and  $h_{min}(t)$  versus  $t$ . Bottom right:  $h_{min}(t - \tilde{t}_1)$  versus  $t - \tilde{t}_1$  where  $h_{min}(\tilde{t}_1) = 1$ .

minimum). Similarly, so long as the maximum is larger than 1 we have  $h^0 < h^1 < h^2 < h^3$  near the maximum, suggesting that the larger  $n$  is, the faster the diffusion will be (near the maximum). This conflict of timescales appears to be mediated through the conservation of mass. Since the mean of the solution is conserved, we find that the solution moves as slowly as its slowest part (which is around the minimum): thus the larger  $n$  is, the slower the diffusion. This is demonstrated in the upper left plot of Figure 16: the  $n = 3$  solution takes longer to relax than the  $n = 0$  solution. Beyond the time  $t_1$  there is no conflict; both the minimum and maximum should relax more slowly as  $n$  increases. We demonstrate this by plotting  $h_{max}$  versus  $t - t_1$  in the bottom left plot of Figure 16.

For  $q = .5$  we compute a  $2\pi$ -periodic steady state  $h_{ss}$  with Bond number  $\mathcal{B} = 0.9817$  and area  $A_{ss} = 7.165$ . This arises from rescaling  $k_\alpha$  with minimum height  $\alpha = 0.2145$  and period  $P_\alpha = 6.168$ . The steady state is linearly unstable (see bifurcation diagram 2b with  $\mathcal{B}P_{ss}^{3-q}A_{ss}^{q-1} = 36.29$ .) As for  $q = 2.5$ , we take initial data  $h_{ss} + .001h_{ss}''$  and exponents  $n = 0, 1, 2$ , and  $3$ .

Again, we find that all four solutions relax to the constant steady state  $\overline{h_{ss}} \equiv 1.140$ ; the apparent heteroclinic orbit is robust under this change in mobility. In the top left plot of Figure 16, we plot  $h_{min}$  and  $h_{max}$  versus time for the four evolutions. We see that the larger the exponent  $n$ , the longer it takes for the solution to relax to the constant steady state.

Since  $\overline{h_{ss}} > 1$ ,  $h_{max}(t) > 1$  for all times and there is a time  $\tilde{t}_1$ , dependent on  $n$ , such that  $h_{min}(t) < 1$  for  $t < \tilde{t}_1$  and  $h_{min}(t) > 1$  for  $t > \tilde{t}_1$ . By the same logic as before, for  $t < \tilde{t}_1$ , the time-scales will be dominated by the dynamics of  $h_{min}$ . This is demonstrated in the upper right plot of Figure 16: the  $n = 3$  solution takes longer to relax than the  $n = 0$  solution. Beyond the time  $\tilde{t}_1$ , however, both the minimum and maximum should relax more *quickly* as  $n$  increases. We demonstrate this by plotting  $h_{min}$  versus  $t - \tilde{t}_1$  in the bottom right plot of Figure 16. There we see the speeds of relaxation reverse, as expected.

For  $q = 2.5$ , we verify as follows that the profile of the solution is not largely affected by the mobility function  $h^n$ . First, we find the four ‘half-times’: the times at which  $h_{min}(t_{1/2}) = .5$ . (The use of .5 is essentially arbitrary.) We find that the four solutions at their half-times differ by only 0.1% in the  $L^\infty$  norm. We find analogous results for  $q = .5$ . This suggests that using  $h_{min}(t)$  to set a time-scale is an effective way of closely correlating two points on two different heteroclinic orbits.

**5.2. Changing the type of singularities.** The choice of mobility coefficients in equation (1),  $h_t = -(h^n h_{xxx})_x - \mathcal{B}(h^m h_x)_x$ , affects whether a positive solution can become zero somewhere in finite time. For example, if  $3.5 < n \leq m < n + 2$  then it cannot: the solution stays positive for all time [8, §4.2]. (Note that  $m < n + 2$  means  $q < 3$ .) On the other hand, if  $m \geq n + 2$  then it is possible that the solution could blow up:  $\|h(\cdot, t)\|_{H^1} \rightarrow \infty$  in finite time. But even then we know from the methods of [9] that if  $3.5 < n \leq m$  then the solution remains positive as long as it exists.

Here, we seek the critical exponent  $n_c(q)$  such that if  $n > n_c(q)$  then positive initial data yield positive solutions for all time, while if  $n < n_c(q)$  it is possible for a positive smooth solution to touch down in finite time (becoming then a nonnegative weak solution). From above, if  $q < 3$  then  $n_c(q) \leq 3.5$ .

For  $q = 1$ , Goldstein et al. [13, §4] presented simulations with  $n = 1$  that suggest a finite-time singularity is possible if  $\mathcal{B} > 1$ . Bertozzi and Pugh presented numerical simulations for  $q = 1$  and  $n = 3$  in which the solutions remain positive for all time and appear to converge to one droplet per period as  $t \rightarrow \infty$  [8]. This suggests that  $1 \leq n_c(1) \leq 3$ .

Here we consider two further  $q$ -values,  $q = 2.5$  and  $q = .5$ . In each case we take initial data  $h_{ss} - .001h''_{ss}$ , with the same steady states  $h_{ss}$  as in §5.1.

We saw for  $q = 2.5$  and  $n = 1$ , in §4.6, that solutions appeared to touch down in finite time, hence  $1 \leq n_c(q) \leq 3.5$ . To further approximate the critical  $n$ -value, we performed simulations with  $n = 1.25, 1.5, 1.55, 1.6, 1.65, 1.6625, 1.675, 1.7, 1.75, 2, 2.25, 2.5, 2.75, 3$ , and 4. Our findings suggest

$$1.65 < n_c(2.5) < 1.6625.$$

In the left plot of Figure 17 we plot  $\log_{10} h_{min}(t)$  versus  $t$  for most of these exponents. If  $h_{min}$  is decreasing at an exponential rate then the graph will be linear at large times. If  $h_{min}$  is decreasing to zero in finite time with an algebraic rate then the graph will go to  $-\infty$  at some finite time, dropping down with a vertical slope. From the plot, if  $n = 2$  (the rightmost graph) then  $h_{min}$  decreases monotonically in time, eventually decreasing with an exponential rate. For  $n = 1.75, 1.7, 1.675$ , or  $1.6625$ ,  $h_{min}$  decreases, then increases, and then ultimately decreases with an exponential rate. The solutions with  $n < 1.6625$  appear to be touching down in finite time. However the  $n = 1.6625$  simulation gives a note of caution; it is possible

that the simulations with  $n < 1.6625$  would run until  $h_{min}$  became quite small but would then increase and ultimately decrease exponentially. Note: all of the simulations were run until the 8192 meshpoint simulation lost resolution, except for the  $n = 1.6625$  simulation which required 65,536 meshpoints to resolve the solution when  $h_{min}$  was at its smallest. We ran the simulations many decades beyond those shown to verify the exponential rate of decrease.

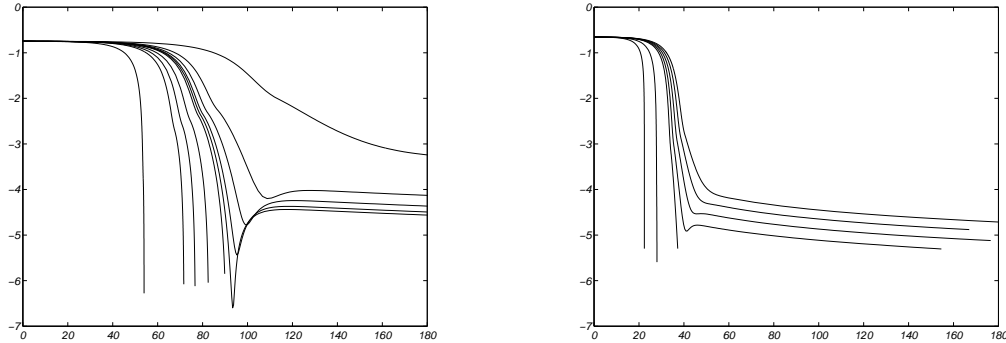


Fig.17:  $\log_{10}(h_{min}(t))$  versus  $t$ . Left:  $q = 2.5$ ;  $n = 1, 1.25, 1.5, 1.55, 1.6, 1.65, 1.6625, 1.675, 1.7, 1.75, 2$ . Right:  $q = .5$ ;  $n = 1, 1.5, 1.8, 1.85, 1.9, 1.95, 2$ .

For  $q = .5$  we similarly considered  $n = 1.25, 1.4, 1.5, 1.55, 1.6, 1.65, 1.7, 1.75, 1.8, 1.85, 1.9, 1.95, 2, 2.25, 2.5, 2.75, 3$ , and 4. We see very similar phenomena to the  $q = 2.5$  case. The right plot of Figure 17 is the analogue of the left plot and suggests that

$$1.8 \leq n_c(.5) < 1.85.$$

For  $n \geq 1.85$ , the solutions stayed positive for the length of the computation and  $h_{min}$  decreased exponentially in time.

**5.3. Splitting singularities.** Our work in §5.1 suggests that heteroclinic orbits can be preserved under some changes of the mobility. On the other hand, qualitative features of a solution can change significantly when the mobility is changed. For example, in §5.2 we demonstrated that the mobility can affect the regularity of the solutions; for sufficiently large  $n$ , solutions are classical for all time while for smaller  $n$ , solutions can become nonnegative weak solutions in finite time. In this section, we demonstrate another effect of changing the mobility: a solution that touches down at one point per period can change into one that touches down at two.

**5.3.1.  $q = 2.5$ .** We first consider  $q = 2.5$  and  $n > 0$ . Then positive periodic smooth solutions of (1) remain bounded in  $H^1$  for as long as they exist:  $\|h(\cdot, t)\|_{H^1} \leq M < \infty$  by [8]. We expect that these solutions will converge to a steady state, as  $t \rightarrow \infty$ . But the positive periodic steady state is linearly unstable, and so we expect solutions to converge either to the constant steady state or to configurations of steady droplets (zero or nonzero contact angle).

As before, we take initial data  $h_{ss} - .001h_{ss}''$  with the same  $h_{ss}$  as in §5.1. In §5.2, we found that if  $n > 1.6625 \approx n_c(2.5)$  then solutions appear to stay positive for all time, with  $h_{min}$  decreasing to zero exponentially slowly in time.

We find for  $n = 1$  that the solution touches down in finite time at one point per period, consistent with a long-time limit of one droplet per period (see left plot of Figure 18). For  $n = 2$  the solution appears to be positive at all times and to touch down at two points per period in the long-time limit (see right plot of Figure 18). This suggests a long-time limit of two steady droplets per period. But it is *impossible* to contain two zero contact angle steady droplets in an interval of length  $2\pi$ , as we argue shortly. In fact, we find that the small ‘proto-droplet’ is actually draining, with its maximum decreasing to zero like  $t^{-.4024}$ . A similar phenomenon was observed by Constantin et al. [12, §III,IV] with  $n = 1$  and  $\mathcal{B} = 0$  (and with different boundary conditions), although their proto-droplet seemed to decay like  $1/t$ . In our case, we find that the draining rate depends on  $n$ .

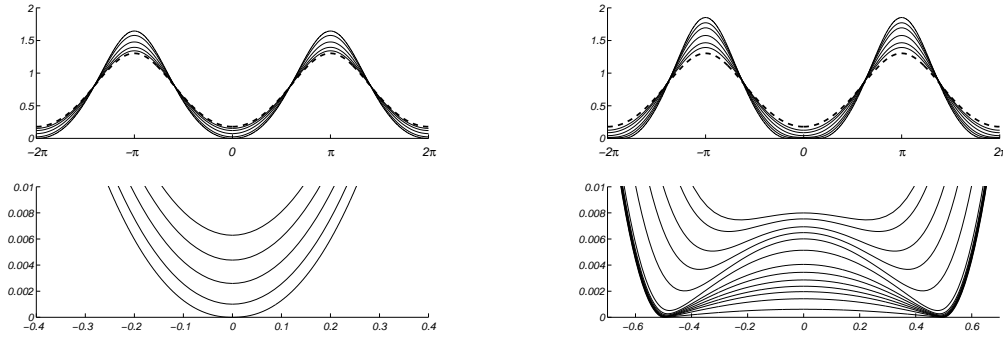


Fig.18:  $q = 2.5$ . Left:  $n = 1$ ;  $h_{min}(t)$  occurs at  $x = 0$ . At all times there appears to be one droplet per period. Right:  $n = 2$ ; at late times, the global minima flank  $x = 0$ , suggesting a long-time limit of two droplets per period. But in fact the smaller droplet appears to be vanishing as  $h_{min} \rightarrow 0$ .

Our simulations suggest that a second critical exponent,  $\tilde{n}_c(q)$ , governs the number of touch-downs per period, at least for the even perturbations we are using. If  $n < \tilde{n}_c(q)$  then there appears to be one touch-down per period, occurring at  $x = 0$ . If  $n > \tilde{n}_c(q)$  then there appear to be two touch-downs per period, with the position of the local minimum moving in time and with the solution being non-symmetric about the local minimum. The singularity splits as  $n$  increases through  $\tilde{n}_c(q)$ . Goldstein et al. [13, §4C] observed something similar for  $h_t = -(hh_{xxx})_x - \mathcal{B}(hh_x)_x$  ( $q = n = m = 1$ ). Specifically, they found a single symmetric singularity that splits into a pair of asymmetric singularities as  $\mathcal{B}$  increases from 1 past  $\mathcal{B} \approx 1.35$ .

We find that

$$1 < \tilde{n}_c(2.5) < 1.25.$$

In the left plot of Figure 19 we plot the late-time profiles for a range of  $n$ . All five profiles shown are the final resolved solution with 8192 meshpoints. In the top plot, we plot the profiles from  $n = 1$  and 1.25. The  $n = 1$  profile has only one local minimum, while the  $n = 1.25$  profile has two. In the bottom plot, we plot the profiles from  $n = 1.5$ , 1.6 and  $n = 1.7$ . Each profile has two local minima, with the distance between the minima increasing with  $n$ .

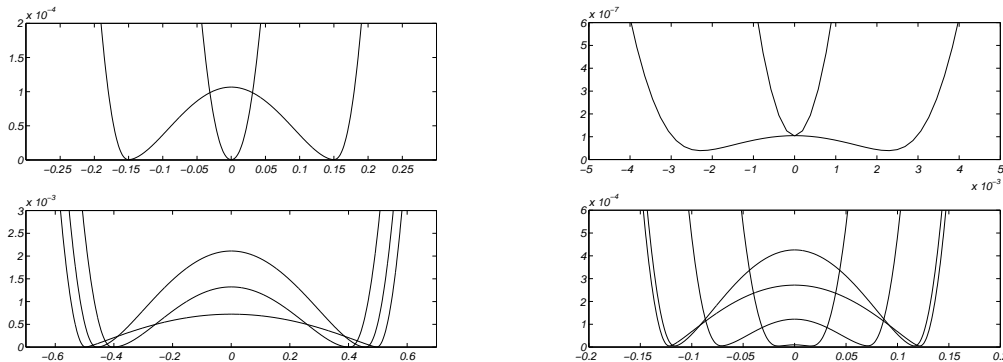


Fig.19: Late-time profiles of  $h$ . Left:  $q = 2.5$ . Top:  $n = 1$  (single minimum) and 1.25. Bottom:  $n = 1.5, 1.6, 1.7$ ; width of proto-droplet increases with  $n$ . Right:  $q = .5$ . Top:  $n = 1$  (single minimum) and 1.25. Bottom:  $n = 1.4, 1.6, 1.8, 2$ ; width of proto-droplet increases with  $n$ .

The  $n = 3$  and 4 evolutions appear to be very similar to the  $n = 2$  evolution. We did not do any simulations beyond  $n = 4$  since the larger the value of  $n$ , the longer the simulation had to run before we could observe anything tangible — the mobility coefficient  $h^n$  is very small near the local minimum, where  $h$  is small. We could not compensate by taking large time-steps, because  $h^n$  could be quite large near the local maximum, since  $h_{max}(t) > 1$ . (Large differences in time-scales are difficult to handle numerically.)

We now prove our earlier claim that for  $q = 2.5$  and  $\mathcal{B} = 1.561$ , there cannot be two disjoint zero contact angle steady droplets in an interval of length  $2\pi$ , if the total area of the droplets is  $A_{ss} = 4.335$  (the area of the initial data in §5.1). There does exist a *single* zero angle droplet steady state with that area and with length less than  $2\pi$  (the length is  $P_{ss} = A_{ss}^{-3} (E_0(2.5)/\mathcal{B})^2 = 5.287 < 2\pi$ ), by [19, Theorem 7]. Hence there *is* a zero contact angle droplet to which the solution on the right of Figure 18 could relax. But if there were a pair of zero contact angle steady state droplets, with areas  $A_1 = \lambda A_{ss}$  and  $A_2 = (1 - \lambda)A_{ss}$ , then the combined length of the two droplets would be

$$P_1 + P_2 = (\lambda^{-3} + (1 - \lambda)^{-3}) A_{ss}^{-3} (E_0(2.5)/\mathcal{B})^2.$$

The righthand side is a convex function of  $\lambda$ , achieving its minimum value 84.5905 at  $\lambda = 1/2$ . This minimum value is greater than  $2\pi$ , and so one cannot fit the two droplet steady states in an interval of length  $2\pi$ . Thus the simulations described earlier cannot be converging to a

pair of steady zero contact angle droplets. Indeed, our computations show the proto-droplet is slowly draining.

5.3.2.  $\mathbf{q} = .5$ . For  $q = .5$  we took initial data  $h_{ss} - .001h''_{ss}$  (for  $h_{ss}$  as in §5.1) and observed phenomena very similar to those in the  $q = 2.5$  case. We find there is an exponent  $\tilde{n}_c(.5)$  such that if  $n < \tilde{n}_c(.5)$  then there is only one touch-down per period and if  $n > \tilde{n}_c(.5)$  then there can be two. Again, our simulations suggest

$$1 < n_c(.5) < 1.25;$$

see the plots to the right of Figure 19. In the right top plot, we present the final resolved solutions for  $n = 1$  and 1.25 with 32,768 meshpoints. The local minima for  $n = 1.25$  are much closer to each other than in the  $q = 2.5$  plot. In fact, at 8192 meshpoints it appeared that there would be only one local minimum; as more time passed it split into two. In the right bottom plot of Figure 19 we plot solutions with  $n = 1.4, 1.6, 1.8,$  and 2. The  $n = 1.4, 1.6,$  and 1.8 solutions are with 8192 meshpoints, and the  $n = 2$  solution is with 16,384 meshpoints. The profiles are all resolved and were chosen to have comparable  $h_{min}$ . The distance between the local minima in the plot increase monotonically with  $n$ .

The evolutions for  $n = 1$  and 2 are very similar to those shown in the plots of Figure 18. Specifically, for  $n = 2$  the long-time limit appears to be one droplet. This is interesting since for  $q = .5$  (unlike for  $q = 2.5$ ), it *is* possible to have two disjoint zero contact angle steady solutions in an interval of length  $2\pi$ , as we now show. We have a Bond number  $\mathcal{B} = 0.9817$  and area  $A_{ss} = 7.165$  (from §5.1). A single zero contact angle steady state would satisfy [17, §3.1]

$$P_{ss} = A_{ss}^{1/5} (E_0(.5)/\mathcal{B})^{2/5},$$

where  $E_0(.5) = 32.86$ . We find  $P_{ss} = 6.038 < 2\pi$ . Thus a single zero contact angle steady state is a potential long-time limit. For two zero contact angle steady states, we find

$$P_1 + P_2 = (\lambda^{1/5} + (1 - \lambda)^{1/5}) A^{1/5} (E_0(.5)/\mathcal{B})^{2/5}.$$

This is a concave function with its maximum at  $\lambda = 1/2$ . We find that  $P_1 + P_2 < 2\pi$  if  $\lambda \leq 10^{-7}$  (approx.) and so one *can* have two zero contact angle droplets — but one of them must be fairly small. For example, if  $\lambda = 10^{-7}$  then the length of the smaller droplet is  $P_1 = 0.2404$ . In the bottom right plot of Figure 19 the profile for  $n = 2$  (the longest proto-droplet shown) has length .2431, which is close to .2404; thus a two-droplet long-time limit is at least a possibility. However, like for  $q = 2.5$ , the proto-droplet appears to shrink in time, with its maximum value decreasing to zero like  $t^{-.4056}$ . (As for  $q = 2.5$ , the draining rate also depends on  $n$ .) We did not succeed in finding a  $q, n,$  and initial data that yield a solution with a multi-droplet configuration as its longtime limit. But we believe it should be possible to find this somehow.

## 6. NUMERICAL METHODS

The numerical simulations are done using a finite-difference evolution code. Throughout this section, the diffusion coefficients are represented as functions  $f$  and  $g$ ; we use power law coefficients  $f(y) = y^n$  and  $g(y) = \mathcal{B}y^m$  in our simulations for this paper. The exponent  $\ell$  represents the  $\ell^{\text{th}}$  time-step and  $h^\ell$  is the numerical approximation of the solution at time  $t_\ell = \ell\Delta t$ .

**6.1. The evolution code.** We use an adaptive time-stepping scheme based on a Crank-Nicolson scheme:

$$\begin{aligned} \frac{h^{\ell+1} - h^\ell}{\Delta t} = & -\frac{1}{2} (f(h^{\ell+1/2})h_{xxx}^{\ell+1})_x - \frac{1}{2} (f(h^{\ell+1/2})h_{xxx}^\ell)_x \\ & -\frac{1}{2} (g(h^{\ell+1/2})h_x^{\ell+1})_x - \frac{1}{2} (g(h^{\ell+1/2})h_x^\ell)_x. \end{aligned}$$

Here the diffusion coefficients are evaluated at  $h^{\ell+1/2}$ , which we find by linearly extrapolating the solutions  $h^{\ell-1}$  and  $h^\ell$  to time  $t_\ell + \Delta t/2$ . The scheme is  $O(\Delta t^2)$  on time intervals where  $\Delta t$  is fixed and is  $O(\Delta t)$  at the time when the timestep is changed. We explain the adaptive timestepping in §6.2.

Finding  $h^{\ell+1}$  reduces to solving a linear problem, which we write in a residual formulation:

$$(10) \quad \mathcal{L}z = -\Delta t [f(h^{\ell+1/2})(h_{xxx}^\ell + r(h^{\ell+1/2})h_x^\ell)]_x$$

where  $z = h^{\ell+1} - h^\ell$  and  $r(y) = g(y)/f(y)$ , and the linear operator  $\mathcal{L}$  is defined by

$$\mathcal{L}z := z + \Delta t \frac{1}{2} [f(h^{\ell+1/2})(z_{xxx} + r(h^{\ell+1/2})z_x)]_x.$$

The scheme uses  $h^{\ell-1}$  and  $h^\ell$  to compute  $h^{\ell+1}$ ; for the first step we take  $h^{-1} = h^0$ .

We now perform a linear stability analysis of the scheme about the constant steady state  $h \equiv \bar{h}$ , for power law coefficients  $f(y) = y^n$  and  $g(y) = \mathcal{B}y^m$ . The linearized equation is  $h_t = -\bar{h}^n h_{xxxx} - \mathcal{B}\bar{h}^m h_{xx}$ . Initial data  $h^0(x) = \varepsilon \cos(kx)$  yields  $h^{\ell+1} = \sigma(k)^{\ell+1} \varepsilon \cos(kx)$  where

$$\sigma(k) = \frac{1 - \frac{\Delta t}{2} \bar{h}^n k^2 (k^2 - \mathcal{B}\bar{h}^{m-n})}{1 + \frac{\Delta t}{2} \bar{h}^n k^2 (k^2 - \mathcal{B}\bar{h}^{m-n})} =: \frac{1 - \mu(k)}{1 + \mu(k)}.$$

Hence there is a band of unstable modes: if  $0 < k^2 < \mathcal{B}\bar{h}^{m-n}$  (*i.e.*  $\mu(k) < 0$ ) then  $|\sigma(k)| > 1$  and the initial data  $h_0(x) = \varepsilon \cos(kx)$  yields a solution that grows exponentially in time. We consider a numerical scheme linearly stable if perturbations *outside* this band are not amplified:

$$k^2 \geq k_c^2 := \mathcal{B}\bar{h}^{m-n} \implies |\sigma(k)| \leq 1.$$

It follows immediately from the form of the growth factor that the Crank-Nicolson scheme is linearly stable, as expected. Such a linear stability analysis provides a useful guide, though

it is directly relevant only for small perturbations of flat steady states.

For the spatial discretization, the key issue is to implement the scheme in a way that preserves steady states. By (3), a steady state  $h_{\text{ss}}$  satisfies  $h_{\text{ss}xxx} + r(h_{\text{ss}})h_{\text{ss}x} = 0$ . Such an ‘analytic steady state’ will not generally be a ‘finite-difference steady state’, although  $h_{\text{ss}}$  will be  $O(\Delta x^2)$ -close to the finite-difference steady state  $\tilde{h}$  satisfying the following discretization:

$$(11) \quad \tilde{h}_{i+2} - 3\tilde{h}_{i+1} + 3\tilde{h}_i - \tilde{h}_{i-1} + \Delta x^2 \frac{r(\tilde{h}_{i+1}) + r(\tilde{h}_i)}{2} (\tilde{h}_{i+1} - \tilde{h}_i) = 0, \quad i = 1 \dots N.$$

The meshpoints are  $x_1 = \Delta x, x_2 = 2\Delta x, \dots, x_N = X$ , where  $X$  is the length of the interval, and we denote the function values at the meshpoints with subscripts:  $\tilde{h}_1, \tilde{h}_2, \dots, \tilde{h}_N$ . The function is periodic:  $\tilde{h}_0 = \tilde{h}_N$ .

To implement the residual formulation (10), we apply the  $O(\Delta x^2)$  approximation

$$(12) \quad [(f(h)(z_{xxx} + r(h)z_x)]_i \simeq \frac{f_{i+}}{\Delta x} \left( \frac{z_{i+2} - 3z_{i+1} + 3z_i - z_{i-1}}{\Delta x^3} + r_{i+} \frac{z_{i+1} - z_i}{\Delta x} \right) - \frac{f_{i-}}{\Delta x} \left( \frac{z_{i+1} - 3z_i + 3z_{i-1} - z_{i-2}}{\Delta x^3} + r_{i-} \frac{z_i - z_{i-1}}{\Delta x} \right),$$

where the subscripts  $i+$  and  $i-$  denote the right-average and left-average, for example:

$$r_{i+} := \frac{r(h_{i+1}^{\ell+1/2}) + r(h_i^{\ell+1/2})}{2}, \quad r_{i-} := \frac{r(h_i^{\ell+1/2}) + r(h_{i-1}^{\ell+1/2})}{2}.$$

This approximation yields a  $O(\Delta x^2)$ -accurate matrix approximation  $\tilde{\mathcal{L}}$  of the operator  $\mathcal{L}$ . Using this, the residual formulation is written

$$\tilde{\mathcal{L}}\vec{z} = R\vec{H}S(h^{\ell-1}, h^\ell).$$

The  $N \times N$  matrix  $\tilde{\mathcal{L}}$  is pentadiagonal periodic. The righthand side of (10) is discretized analogously.

It follows immediately from the condition (11) for a finite difference steady state that the above time-stepping scheme preserves finite-difference steady states. To ensure this we factored  $f$  out in (12) before doing the finite-difference approximation of  $f(h)h_{xxx} + g(h)h_x$ , because the relation  $fr = g$  does not hold in the discrete setting:  $f_{i+}r_{i+} \neq g_{i+}$  for example. Also, by factoring  $f$  out we have also isolated the pressure gradient term,  $(h_{xx} + \mathcal{B}/qh^q)_x$ , in the equation.

**6.2. Timestepping and accuracy.** The adaptive timestepping controls the accuracy as follows. An error tolerance is set,  $\varepsilon = 10^{-11}$ . At each time step, we first use the Crank-Nicolson scheme to compute  $h_1$ , an approximation of the solution at time  $t + \Delta t$ . We then take two timesteps with  $\Delta t/2$  to compute  $h_2$ , another approximation of the solution at time  $t + \Delta t$ . For some constant  $C$ , the error is bounded [16, §5.2] by the difference of  $h_1$  and  $h_2$ :

$$\|h(\cdot, t + \Delta t) - h_2\|_\infty \leq C\|h_1 - h_2\|_\infty.$$

If  $\|h_1 - h_2\|_\infty > \varepsilon$  then we replace  $\Delta t$  with  $\Delta t/2$  and try again (without advancing in time). If  $\|h_1 - h_2\|_\infty < \varepsilon/10$  then we replace  $\Delta t$  with  $2\Delta t$  and try again. If  $\|h_1 - h_2\|_\infty$  lies between  $\varepsilon$  and  $\varepsilon/10$  then we take the solution at time  $t + \Delta t$  to be  $h_2$ .

Adaptive timestepping takes at least three times longer than using the Crank-Nicolson scheme with a fixed timestep. For this reason, we performed all of our exploratory studies using a fixed time-step. Once we found phenomena of interest, we re-ran using adaptive time-stepping. Since the first time-step has  $O(\Delta t^2)$  local truncation error, rather than  $O(\Delta t^3)$ , the adaptive time-stepper initially refines  $\Delta t$  to meet the tolerance. Also, most runs had an initial fast transient (see §4.1.1) which required early refinement of the timestep.

Admittedly, since we do not know the constant  $C$  this error control is valid only as long as  $C$  is not large. In practice we find that, after the initial transient, the timestep is rarely reduced, except near times when the run has to be stopped anyway in order to point-double.

**6.3. Computing the finite-difference steady state.** Here, we only discuss the case of power law coefficients. Given  $N$  uniformly distributed meshpoints between 0 and  $X = 2\pi$ , we seek a finite-difference steady state  $\tilde{h}$  that solves the  $N$  equations (11) to the level of round-off error.

We solve the  $N$  equations (11) simultaneously using Newton-Raphson iteration. To do this, we need a good first guess for  $\tilde{h}$ . In the following, we describe how we find a first guess and then how we execute the Newton-Raphson iteration.

Given the exponent  $q \neq 0$  we first compute the rescaled steady state  $k = k_\alpha$  at the  $N$  points  $x = P/N, 2P/N, \dots, P$ . As described in [17, §6.1], we do this by viewing the steady state equation

$$(13) \quad k_{xx} + \frac{k^q - 1}{q} = 0, \quad k(0) = \alpha, \quad k_x(0) = 0,$$

as an initial value problem in  $x$ . We verify that  $k$  is spectrally accurate by using a discrete fast Fourier transform to check that the power-spectrum is fully resolved. Since for numerical purposes,  $k$  is an exact solution of equation (13), in the following we refer to it as an ‘analytic steady state’.

Once the analytic steady state  $k$  is known, we rescale it to find an analytic steady state  $h_{ss}$  of period  $2\pi$ , by taking  $D = 1$  in the rescaling [19, eq. (7)] and defining

$$\mathcal{B} = \left(\frac{P}{2\pi}\right)^{2q}, \quad \text{and} \quad h_{ss} = \left(\frac{1}{\mathcal{B}}\right)^{1/q} k.$$

This gives  $h_{ss}$  at  $N$  meshpoints. By construction,  $h_{ss}$  is an analytic steady state for  $(h_{ss})_{xx} + (\mathcal{B}h_{ss}^q - 1)/q = 0$  with period  $2\pi$ .

To find the finite-difference steady state  $\tilde{h}$  close to  $h_{\text{ss}}$  we need to solve the  $N$  equations (11), which we write as

$$\vec{F}(\tilde{h}) := M\tilde{h} + \vec{V}(\tilde{h}) = \vec{0}$$

where  $M$  is a tetradiagonal periodic matrix and  $\vec{V}(\tilde{h})_i$  is a nonlinear function of  $\tilde{h}_i$  and  $\tilde{h}_{i+1}$ . The Newton–Raphson iteration is

$$\tilde{h}^{\text{new}} = \tilde{h}^{\text{old}} - (D\vec{F}(\tilde{h}^{\text{old}}))^{-1}\vec{F}(\tilde{h}^{\text{old}}).$$

To iterate, one has to solve  $D\vec{F}\vec{x} = \vec{F}(\tilde{h}^{\text{old}})$ . We find that  $D\vec{F}$  is a singular matrix of rank  $N - 1$ . We solve  $D\vec{F}\vec{x} = \vec{F}(\tilde{h}^{\text{old}})$  using the singular value decomposition of  $D\vec{F}$  obtained using LAPACK’s ‘dgesvd.f’ to solve for  $\vec{x}$ . The iteration is then started with the initial guess  $h_{\text{ss}}$  and stopped when the largest error in the  $N$  equations (11) is less than  $10^{-14}$ .

In a different approach, one might attempt to compute the finite difference steady state  $\tilde{h}$  with a relaxation method, by computing the finite-difference solution of the evolution equation  $h_t = \Delta h + (\mathcal{B}h^q - 1)/q$  for large  $t$ . This seems unlikely to succeed because steady states of this PDE have the same linear stability properties (with respect to zero–mean perturbations) as the steady states we are trying to compute, making it extremely difficult to obtain convergence to linearly unstable steady states.

*Note:* For  $q = 1$ , the finite–difference steady states satisfy a linear problem:

$$\tilde{h}_{i+2} - 3\tilde{h}_{i+1} + 3\tilde{h}_i - \tilde{h}_{i-1} + \Delta x^2 \tilde{\mathcal{B}} (\tilde{h}_{i+1} - \tilde{h}_i) = 0, \quad i = 1 \dots N.$$

In §4.3, we perturb a nontrivial  $2\pi$ -periodic finite-difference steady state. This will be close to an analytic steady state. Even analytic steady states are  $a + b \cos(\sqrt{\mathcal{B}}x)$  and are  $2\pi$ -periodic if  $\sqrt{\mathcal{B}}$  is an integer. Sampling such a steady state on a uniform mesh gives

$$\tilde{h}_j = a + b \cos(\sqrt{\mathcal{B}} j \Delta x),$$

and one can check that  $\tilde{h}$  is a finite–difference steady state provided

$$\tilde{\mathcal{B}} = 2 \frac{1 - \cos(\sqrt{\mathcal{B}}\Delta x)}{\Delta x^2} = \mathcal{B} - O(\Delta x^2).$$

That is, there are nontrivial analytic steady states for a countable collection of Bond numbers,  $\mathcal{B} \in \{1^2, 2^2, 3^2, \dots\}$ , and nontrivial finite difference steady states for a nearby countable set of Bond numbers  $\tilde{\mathcal{B}}$ .

**6.4. Stopping criteria and issues for singularities.** To test whether to stop the code, we compute the minimum value of  $h^\ell$  at each time-step. If this minimum is ever less than or equal to zero, we stop the code. As discussed in §§4 and 5, we find that the stopping criterion is indeed often met. While this suggests a finite-time singularity, we emphasize that the code has not been written in a way to carefully resolve such singularities — the singularity may occur in infinite time, with the stopping criterion being met in finite time

because of instabilities causing oscillations in the profile. In practice, the stopping criterion was always met after the solution became spectrally unresolved.

The code was designed to preserve the periodic steady states, rather than being written to preserve positivity. (There are a number of different approaches to ensuring positivity: we refer interested readers to [1, 14, 28].) For this reason, it might be that the code is stopping spuriously. Also, as the code has no local mesh refinement, we have to over-resolve much of the solution in order to resolve the solution where it is tending to zero. This over-resolution away from the singular points slows the computation significantly.

That being said, we use the code primarily to study nonsingular behavior. Some of our results are suggestive of finite-time singularities; we present them with the above caveats. To find fine details of the temporal and spatial scales of the singularities, we would implement a code that preserves positivity and has an adaptive spatial mesh.

Finally, we are not using a fully-implicit timestepping scheme; a basic such scheme would only be  $O(\Delta t)$  but could be made  $O(\Delta t^2)$  using Richardson extrapolation [12]. It would likely be very stable, but slow. For speed, we chose a *partially* implicit scheme and then checked for numerical instabilities when we held the timestep fixed. We observed none. Also, it seems unlikely that our adaptive timestepper was taking small timesteps in order to control numerical instabilities, since after the initial transient, the timesteps were refined only when the solution was becoming singular.

## 7. CONCLUSIONS AND FUTURE DIRECTIONS

We have shown numerically for the evolution equation  $h_t = -(h^n h_{xxx})_x - \mathcal{B}(h^m h_x)_x$  that our linear stability theorems in [18] accurately predict the short-time nonlinear behavior of the solutions near positive periodic and constant steady states. We have found strong evidence for the existence of heteroclinic connections between steady states, as suggested by our theorems on the energy levels of steady states [19]. We have further observed a mountain pass scenario in which perturbations of a periodic steady state relax towards either a droplet or a constant steady state.

All of this suggests that the energy landscape through which the solutions travel is fairly simple, and that understanding the relative energy levels of the steady states gives considerable insight into that landscape.

It is worth recalling that the evolution equation (1) describes *gradient flow* for the energy  $\mathcal{E}$  defined in (2), with respect to the following weighted  $H^{-1}$  inner product. Let  $h(x, t)$  be a positive smooth function that is  $X$ -periodic in  $x$ , and for each  $t$ , define an inner product on functions  $a, b \in C(\mathbb{T}_X)$  having mean value zero by

$$\langle a, b \rangle := \int_0^X A'(x)B'(x)h(x, t)^n dx,$$

where  $A, B \in C^2(\mathbb{T}_X)$  satisfy  $(h^n A_x)_x = a$  and  $(h^n B_x)_x = b$ . Then the equation (1) is equivalent to:

$$\frac{\delta \mathcal{E}}{\delta \phi} = -\langle h_t, \phi \rangle \quad \text{for all } \phi \in C(\mathbb{T}_X) \text{ having mean value zero.}$$

Hence the variation of the energy is most negative in the direction  $\phi = h_t$ , so that the evolution equation for  $h(x, t)$  simply describes flow by steepest descent on the energy surface of  $\mathcal{E}$ , with respect to the inner product  $\langle \cdot, \cdot \rangle$ . Note that this inner product is *time-dependent* since it depends on  $h^n$ , *i.e.* on the solution itself.

The above gradient flow formulation with weighted  $H^{-1}$  inner product was observed by Taylor and Cahn [23]; their evolution (7a) contains our equation (1). For the special case of the Cahn–Hilliard equation the inner product is unweighted, since the fourth order term in the equation is linear. Gradient flow ideas for related equations have been used in [4, 26], and a Wasserstein–flow idea in [22].

In §5 we presented numerical results on the persistence of heteroclinic connections under changes in the mobility parameters  $n$  and  $m$ . There we changed  $n$  and  $m$  in a way that preserved  $q = m - n + 1$ , and thus preserved the energy  $\mathcal{E}$  and also the steady states (which are critical points of the energy). Hence our change in mobilities does not change the energy landscape. But it does change the weight  $h^n$  appearing in the inner product  $\langle a, b \rangle$  and in the equations for  $A$  and  $B$ , and this is how changing the mobility affects the evolution. In §5 we found the *timescale* of the solution changed noticeably in response to changes in the mobilities, even though the *shape* of the solution changed little.

Lastly, in §5 we further investigated *critical* mobility exponents, such as the critical  $n$  above which solutions remain positive for all time (in other words, the critical exponent for film rupture or pinch-off). An interesting question for the future is to find formulas for the critical mobility exponents. These critical exponents determine important qualitative features of the evolution and determining them would shed considerable light not only on the equation (1) studied here, but also on related equations that arise from physical models.

**Acknowledgments.** Laugesen was partially supported by NSF grant number DMS-9970228, and a grant from the University of Illinois Research Board. He is grateful for the hospitality of the Department of Mathematics at Washington University in St. Louis.

Pugh was partially supported by NSF grant number DMS-9971392, by the MRSEC Program of the NSF under Award Number DMR-9808595, by the ASCI Flash Center at the University of Chicago under DOE contract B341495, and by an Alfred P. Sloan fellowship. The computations were done using a network of workstations paid for by an NSF SCREMS grant, DMS-9872029. Part of the research was conducted while enjoying the hospitality of the Mathematics Department and the James Franck Institute of the University of Chicago.

Pugh thanks Todd Dupont and Bastiaan Braams for illuminating conversations regarding numerical issues.

#### REFERENCES

- [1] J. W. Barrett, J. F. Blowey, and H. Garcke. Finite element approximation of a fourth order nonlinear degenerate parabolic equation. *Numer Math*, 80(4):525–556, 1998.
- [2] E. Beretta, M. Bertsch, and R. Dal Passo. Nonnegative solutions of a fourth order nonlinear degenerate parabolic equation. *Arch Ration Mech Anal*, 129:175–200, 1995.
- [3] F. Bernis and A. Friedman. Higher order nonlinear degenerate parabolic equations. *J Diff Eq*, 83:179–206, 1990.
- [4] A. J. Bernoff, A. L. Bertozzi and T. P. Witelski. Axisymmetric surface diffusion: dynamics and stability of self-similar pinchoff. *J Statist Phys*, 93(3–4), 725–776, 1998.
- [5] A. L. Bertozzi, M. P. Brenner, T. F. Dupont, and L. P. Kadanoff. Singularities and similarities in interface flow. In L. Sirovich, editor, *Trends and Perspectives in Applied Mathematics*, volume 100 of *Applied Mathematical Sciences*, pages 155–208. Springer–Verlag, New York, 1994.
- [6] A. L. Bertozzi and M. Pugh. The lubrication approximation for thin viscous films: the moving contact line with a ‘porous media’ cut off of van der Waals interactions. *Nonlinearity*, 7:1535–1564, 1994.
- [7] A. L. Bertozzi and M. Pugh. The lubrication approximation for thin viscous films: regularity and long time behavior of weak solutions. *Commun Pur Appl Math*, 49(2):85–123, 1996.
- [8] A. L. Bertozzi and M. C. Pugh. Long–wave instabilities and saturation in thin film equations. *Commun Pur Appl Math*, 51:625–661, 1998.
- [9] A. L. Bertozzi and M. C. Pugh. Finite–time blow–up of solutions of some long–wave unstable thin film equations. *Indiana Univ Math J*, to appear, 2000.
- [10] A. L. Bertozzi and M. C. Pugh. Presented at 1997 APS Division of Fluid Dynamics meeting.
- [11] J. Bricmont, A. Kupiainen, and J. Taskinen. Stability of Cahn–Hilliard fronts. *Commun Pur Appl Math*, 52(7):839–871, 1999.
- [12] P. Constantin, T. F. Dupont, R. E. Goldstein, L. P. Kadanoff, M. J. Shelley and S.-M. Zhou. Droplet breakup in a model of the Hele–Shaw cell. *Phys Rev E*, 47(6):4169–4181, 1993.
- [13] R. Goldstein, A. Pesci, and M. Shelley. Instabilities and singularities in Hele–Shaw flow. *Phys Fluids*, 10(11):2701–2723, 1998.
- [14] G. Grün and M. Rumpf. Nonnegativity preserving convergent schemes for the thin film equation. *Numer Math*, to appear, 2000.
- [15] G. Grün and M. Rumpf. Simulation of singularities and instabilities arising in thin film flow. Submitted to *Euro J Appl Math*, 2000.
- [16] A. Iserles. *A first course in the numerical analysis of differential equations*. Cambridge University Press, Cambridge, 1996.
- [17] R. S. Laugesen and M. C. Pugh. Properties of steady states for thin film equations. *European J Appl Math*, to appear, 2000.
- [18] R. S. Laugesen and M. C. Pugh. Linear stability of steady states for thin film and Cahn–Hilliard type equations. *Arch Ration Mech Anal*, to appear, 2000.
- [19] R. S. Laugesen and M. C. Pugh. Energy levels of steady states for thin film type equations. Preprint, 2000.
- [20] P. Manneville. *Dissipative structures and weak turbulence*. Academic Press Inc., Boston, MA, 1990.
- [21] A. Oron and S. G. Bankoff. Dewetting of a heated surface by an evaporating liquid film under conjoining/disjoining pressures. *J Colloid Interface Sci*, 218:152–166, 1999.
- [22] F. Otto. Lubrication approximation with prescribed non–zero contact angle: an existence result. *Commun Part Diff Eq*, 23:2077–2164, 1998.
- [23] J. E. Taylor and J. W. Cahn. Linking anisotropic sharp and diffuse surface motion laws via gradient flows. *J Stat Phys*, 77(1-2):183–197, 1994.
- [24] M. B. Williams and S. H. Davis. Nonlinear theory of film rupture. *J Colloid Interf Sci*, 90(1):220–228, 1982.
- [25] T. P. Witelski and A. J. Bernoff. Stability of self-similar solutions for van der Waals driven thin film rupture. *Phys Fluids*, 11(9):2443–2445, 1999.
- [26] T. P. Witelski and A. J. Bernoff. Dynamics of three–dimensional thin film rupture. Preprint, 2000.

- [27] W. W. Zhang and J. R. Lister. Similarity solutions for van der Waals rupture of a thin film on a solid substrate. *Phys Fluids*, 11(9):2454–2462, 1999.
- [28] L. Zhornitskaya and A. Bertozzi. Positivity preserving schemes for lubrication-type equations. *SIAM J Numer Anal*, 37(2):523–555, 2000.

EMAIL CONTACT: laugesen@math.uiuc.edu, mpugh@math.upenn.edu

DEPARTMENT OF MATHEMATICS, UNIVERSITY OF ILLINOIS, URBANA, IL 61801

DEPARTMENT OF MATHEMATICS, UNIVERSITY OF PENNSYLVANIA, PHILADELPHIA, PA 19104